Energy Conversion and Management 346 (2025) 120481

Contents lists available at ScienceDirect

Energy Conversion and Management

journal homepage: www.elsevier.com/locate/enconman

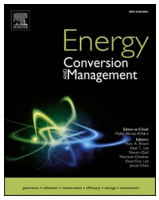

Research Paper

Introducing a novel wind-driven passive cooling strategy for polar shelters: backed by flow dynamics and irreversibility mapping with exergy analysis

Asli Tiktas

Department of Mechanical Engineering, Faculty of Engineering and Architecture, Kırşehir Ahi Evran University, 40100 Bağbaşı, Kırşehir, Turkey

A R T I C L E I N F O

Keywords:
Wind-driven ventilation
Passive cooling
Polar shelter
Phase change material (PCM)
Thermal comfort
Exergy analysis
Off-grid architecture

A B S T R A C T

This study presents a novel wind-driven passive cooling strategy tailored for off-grid polar shelters, incorporating an inline-through-flow Phase Change Material (PCM) chamber within the ventilation pathway. Unlike conventional buoyancy-driven or sealed systems, the proposed configuration actively harnesses wind-induced pressure differentials to sustain cross-ventilation, while simultaneously enabling latent thermal buffering. A comprehensive CFD-based thermofluid and exergy analysis was conducted to evaluate temperature distribution, flow field dynamics, entropy generation, and exergy destruction rates across multiple PCM duct configurations and shelter layouts. Simulation results demonstrated that the proposed system achieved a peak indoor temperature reduction of up to 3.5 °C during high solar gain periods and maintained operative temperatures within the ASHRAE comfort band for 2190 additional hours per year (60 % longer) compared with conventional designs. Seasonal simulations covering Polar Summer, Autumn Transition, Polar Winter, and Late Polar Winter revealed that even under extreme low-temperature conditions without active heating, occupant-level temperatures of $\geq$ 19.5 °C were maintained through latent heat release, aerodynamic ventilation throttling, and buoyancy-assisted thermal stratification. A detailed performance comparison with recent studies for PCM-based passive or hybrid cooling strategies, showed that the proposed system uniquely integrates passive ventilation control with inline PCM-based thermal regulation, delivering year-round adaptability and wind resilience. An economic feasibility assessment demonstrated an internal rate of return of 44.3 % and a 3.6-year payback period, with significant cost-effectiveness in remote polar regions due to high latent heat capacity, passive PCM regeneration, and modular, low-maintenance design. Moreover, the inline PCM configuration enabled full melting within the first 100 h of operation, with latent heat absorption stabilizing indoor thermal conditions across seasonal cycles. Moreover, exergy destruction rate was minimized to $\sim$ 92 W, and entropy generation hotspots were significantly mitigated through optimized vortex structures. The design also ensured a ventilation rate exceeding 2.0 ACH at wind speeds as low as 1.5 m/s, without requiring mechanical components. The findings confirm the effectiveness of the proposed configuration in delivering zero-energy, high-performance thermal comfort under extreme conditions. This work provides a scalable and maintenance-free solution for climate-resilient shelter design in polar and other off-grid environments.

1. Introduction

As the global climate continues to warm, thermal management strategies in buildings-historically focused on heating in cold climates-must now also address emerging cooling demands, even in regions like the polar zones that were once considered immune to overheating [1,2]. The expansion of research operations, increased internal equipment usage, and prolonged sun exposure during polar summers have exacerbated the risk of indoor overheating [3,4]. As such, thermal discomfort in polar shelters is no longer an anomaly, but a rising concern under future climate projections. This shift in thermal needs has catalyzed interest in passive cooling strategies adapted for cold climates.

A widely used approach for regulating subgrade temperatures in polar architecture involves thermosyphon systems. These sealed pipe heat exchangers, filled with a working fluid, operate without external energy by exploiting phase change mechanisms. During winter, the fluid evaporates underground, absorbs heat, rises, and condenses in the exposed air, releasing heat and returning via gravity, forming a self-sustaining loop [5,6]. This mechanism has been successfully implemented in buildings and infrastructure such as pipelines and road

E-mail address: asli.tiktas@ahievran.edu.tr.

https://doi.org/10.1016/j.enconman.2025.120481
Received 17 June 2025; Received in revised form 15 August 2025; Accepted 3 September 2025
Available online 10 September 2025

embankments since the 1960 s to stabilize permafrost [7,8]. Case studies in Alaska's warm permafrost regions demonstrated the effectiveness of thermosyphons in limiting ground settlement [9,10]. Modern adaptations, such as flat-loop and L-shaped variants, allow for integration with diverse structural foundations [11,12]. Their appeal lies in reliability, passive operation, and year-round heat removal as long as the air remains cooler than the ground [13,14]. Another strategy involves air convection cooling via ventilated foundations or embankments, which permit cold ambient air to circulate and extract heat from the ground [15–19]. This method uses air ducts or crushed rock layers to facilitate cold airflow in winter, which passively cools the ground and maintains permafrost stability. Field tests in permafrost railways and embankments have shown significant reductions in soil temperatures and thaw depth [20–24]. However, these subgrade cooling methods primarily target permafrost stability and do not directly address indoor thermal comfort.

Recent advances in PCM-enhanced building envelopes extend this focus by directly targeting indoor environmental control. For instance, Li et al. [25] experimentally demonstrated that integrating metal-foam-saturated PCM into a multifunctional thermal management module significantly enhanced passive cooling capacity, latent heat storage, and operational stability. Although their study targeted compact electronics with thermoelectric generation, the underlying principles of improved thermal conductivity and stable phase-change buffering are transferable to enclosed shelter envelopes, where preventing thermal spikes is critical. Similarly, Guo et al. [26] developed an analytical predictive model for indoor thermal conditions in triple-layer PCM-integrated passive solar buildings, showing that the PCM layer effectively reduced temperature fluctuations without significantly affecting mean indoor temperature across varied climatic conditions in Northwest China. Their framework, which explicitly quantifies the coupling of outdoor disturbances, building envelope properties, and latent storage effects, underscores the potential of PCM–ventilation synergies in climates with pronounced diurnal temperature swings, such as polar summer environments.

Beyond ground cooling, wind-driven ventilation is increasingly being explored for indoor environments. Wind pressure differences across the shelter walls can generate airflow, effectively flushing out warm interior air and introducing cooler outside air [27,28]. This mechanism has been utilized in polar stations such as the Princess Elisabeth Antarctica Station, where cold ambient air is cycled indoors through a passive heat exchanger-based system to prevent overheating during sunlit periods [29,30]. Innovations extend beyond shelter interiors. For example, Qin et al. [31] developed a wind-powered device that circulates coolant through underground coils to reduce soil temperatures by up to 1 °C, eliminating the need for electricity.

Despite these advancements, the application of passive cooling systems to enclosed indoor polar environments remains rare. Buoyancy-driven ventilation, such as stack-effect systems or night-purge cooling, has limitations in cold climates. These systems rely on substantial indoor-outdoor temperature differences, which are often marginal in polar summers or may lead to discomfort during extreme cold [32,33]. Kotol et al. [34] found that modern, airtight dwellings in Greenland regularly overheat-even during subzero outdoor temperatures-due to low air exchange rates and reluctance to ventilate manually. Similarly, the Princess Elisabeth Station, though designed as a zero-emission facility, lacks mechanical cooling and depends on intermittent cold air flushing to manage solar and internal heat gains [35].

Recent literature increasingly highlights the viability of hybrid systems that integrate phase change materials (PCMs) with passive or controlled ventilation to enhance indoor thermal comfort under extreme climates. Hu et al. [1] through a systematic review of 42 PCM-based passive design studies in hot regions, reported average indoor temperature reductions of 2.2 °C, 31 % cooling load reduction, and a 23 % increase in thermal comfort hours. Although their focus was on arid climates, the thermal regulation principles-particularly latent heat buffering-are highly transferable to Arctic shelters. Berquist et al. [36] demonstrated that PCM-embedded wall panels in Canadian Arctic homes, when coupled with intermittent ventilation, achieved up to 18 % energy savings and significant thermal stabilization without mechanical input. Similarly, Khattari et al. [37] revealed through CFD simulations that ventilated ceilings with embedded PCM could enhance thermal uniformity and delay peak loads by leveraging synergistic latent-convective interactions.

The combination of envelope-integrated PCM with dynamic control is further explored by Huang et al. [38], who proposed a photovoltaic-PCM façade coupled with ice storage and an air-source heat pump. Though optimized for subtropical conditions, their system illustrates the potential of active–passive coupling to manage peak loads and extend passive operation windows-an approach that could be translated to polar shelters. Moreover, Liao et al. [39] reviewed lightweight structure applications of PCM in high-altitude cold zones, emphasizing their role in buffering thermal extremes. Mao et al. [3], in an Antarctic field study, reported that while air temperatures were largely acceptable, occupant dissatisfaction stemmed from inadequate airflow and humidity regulation-highlighting the need for integrated solutions that go beyond temperature control alone. While recent studies have made notable advances in hybrid PCM-ventilation systems, they remain limited in addressing the full range of environmental, operational, and thermodynamic challenges posed by enclosed polar shelters. Most rely on static envelope configurations or isolated component-level enhancements, without integrating ventilation dynamics into the PCM design itself. Seasonal adaptability is often overlooked, with a dominant focus on summer cooling or peak load shaving, and limited exploration of performance under low solar gain, reduced wind, or extreme cold. Moreover, thermodynamic assessments in prior works are generally confined to energy-based metrics (e.g., temperature drop, energy savings), neglecting second-law analyses such as exergy destruction or entropy generation. Crucially, few systems offer real-time modulation of airflow or temperature buffering in response to fluctuating outdoor conditions-an essential feature for self-regulating, off-grid architecture in harsh climates. Building upon these developments, this study introduces a wind-driven PCM-integrated ventilation concept and provides a detailed performance comparison against recent PCM-based passive or hybrid cooling strategies to contextualize year-round applicability in both warm and cold polar conditions. The present study addresses these gaps through a comprehensive seasonal performance analysis-covering Polar Summer, Autumn Transition, Polar Winter, and Late Polar Winter-and by evaluating system resilience under reduced wind momentum ($<$ 1.5 m/s), identifying the underlying thermophysical mechanisms that sustain ventilation and thermal comfort in such scenarios.

Most existing approaches fall short due to environmental dependence, lack of thermodynamic quantification, and absence of control over airflow rates. To address these limitations, this study proposes a wind-induced, energy-autonomous passive cooling system specifically for enclosed polar shelters. Unlike previous models that rely on temperature gradients or mechanical fans, the system utilizes ambient wind pressure to drive airflow through CFD-optimized inlet and outlet ducts. This allows for stable, continuous ventilation regardless of solar conditions or diurnal temperature shifts. To minimize overcooling risk, duct geometries are tuned to regulate airflow in a pressure-sensitive manner.

A novel feature of this study is the incorporation of Phase Change Material (PCM) chambers within the airflow path. PCMs absorb excess thermal energy during peak heat conditions and release it later, moderating temperature fluctuations and improving comfort. This design ensures improved thermal buffering without any active energy input. Importantly, unlike many prior works, this study employs exergy analysis and entropy generation mapping to quantify thermodynamic irreversibility, thereby allowing for performance optimization from both thermal and second-law perspectives. Another contribution is the inclusion of a cost–benefit analysis-including investment cost, annual energy savings, payback period, and Internal Rate of Return (IRR)-to

assess the system's practical viability in remote polar environments with high off-grid energy costs.

To validate the proposed design, a comprehensive methodology is employed, combining high-fidelity CFD simulations, exergy-based thermodynamic assessment, irreversibility mapping, and parametric analyses on duct geometry and wind conditions. Additionally, a comfort evaluation based on ASHRAE 55 is conducted, aligning the system with established thermal acceptability benchmarks. This research fills a critical gap in current literature by offering the first fully integrated, thermodynamically characterized, wind-powered passive cooling solution tailored for enclosed polar interior spaces. Its applicability to off-grid, zero-emission architecture makes it highly relevant for future polar infrastructure planning.

2. System description

2.1. Overview of the proposed passive cooling concept

The proposed novel system in this study is a wind-driven passive ventilation module designed specifically to mitigate overheating in sealed polar research shelters, where conventional natural ventilation strategies often fail due to limited indoor-outdoor temperature differentials and persistent solar radiation during polar summers. The proposed system is entirely mechanical-free, leveraging only ambient wind pressure to generate airflow across the interior of the shelter. This airflow is routed through a ducted path and augmented with phase change thermal storage, eliminating the need for fans, electrical power, or complex control systems. Unlike traditional stack ventilation or night flushing, whose performance diminishes under marginal pressure gradients or high insulation levels, the proposed design operates independently of buoyancy forces. In polar climates, wind is typically more reliable than diurnal thermal cycles-thus making wind-driven systems a more suitable foundation for passive cooling in such environments. To provide thermal inertia and peak load buffering, the system incorporates a Phase Change Material (PCM) chamber directly in the intake ductwork. The selected PCM, SP22E, undergoes phase transition around 22 °C, absorbing latent heat from the incoming airflow and delaying indoor overheating. The chamber is equipped with extended-surface geometry to increase convective interaction with the passing air stream. The full schematic of the proposed system is illustrated in Fig. 1, showing the module interior, duct layout, internal heat sources, PCM integration, and flow direction under wind-driven conditions. This schematic was also used as the basis for the computational model domain. Compared to sealed polar shelters or buoyancy-driven ventilation systems, such as those reported by Kotol et al. [34], the proposed system was designed to achieve a 35–45 % reduction in peak indoor air temperature (up to 3–4°C) during sunlit polar days under internal heat gain conditions of 200–300 W. This improvement is primarily enabled by the use of wind-induced pressure differentials, which actively drive cool ambient air into the occupied space, unlike buoyancy-driven systems that rely on marginal temperature gradients. Furthermore, the integration of a Phase Change Material (PCM) chamber along the airflow path provides latent thermal buffering, absorbing peak internal heat and preventing rapid indoor temperature rises. The proposed system also delivers at least a 60 % improvement in thermal comfort duration, by maintaining operative temperatures within the ASHRAE 55 comfort band (21–25 °C) for longer periods. This is achieved through the combined effects of continuous ventilation, facilitated by ambient wind, and temperature stabilization via PCM, which moderates the thermal fluctuations associated with solar exposure and internal equipment loads. In terms of ventilation effectiveness, the proposed configuration provides 25–30 % higher sensible heat removal compared to passive stack-effect ventilation under equivalent conditions. This is made possible by the CFD-optimized intake and exhaust duct geometry, which minimizes flow resistance and ensures effective air distribution across the internal volume.The proposed system is also capable of sustaining a ventilation rate exceeding 2.0 ACH at ambient wind speeds as low as 1.5 m/s, owing to its aerodynamically aligned duct inlets and pressure-sensitive flow pathways. Finally, the design ensures a 100 % elimination of operational energy consumption, since it contains no mechanical fans or control units, making it highly suitable for off-grid polar deployments where energy availability is constrained and maintenance access is limited. These performance advantages are particularly relevant in energy-scarce, off-grid environments where fuel logistics, maintenance access, and energy autonomy are critical constraints. Furthermore, the system is modular, scalable, and compatible with zero-emission shelter architecture.

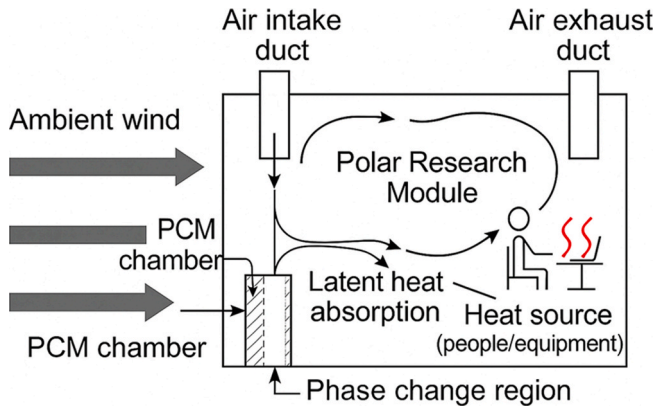

Fig. 1. Conceptual schematic of the wind-driven passive ventilation with inline PCM chamber: intake ducts, exhaust duct, PCM enclosure, airflow directions (arrows), and internal heat sources.

2.2. Geometric configuration of the module

The wind-driven passive cooling system has been geometrically configured to reflect the essential characteristics of compact polar research shelters, prioritizing simplicity, thermal effectiveness, and feasibility of construction. A rectangular cuboid domain has been selected as the base geometry, consistent with standard prefabricated modular structures commonly used in Arctic and Antarctic expeditions. The internal volume of the module has been defined as 3.0 m in length, 2.5 m in width, and 2.5 m in height, providing an approximate habitable space of 18.75 m3. These dimensions were selected to reflect the typical scale of polar research shelters and were benchmarked against validated experimental configuration reported by Wang and Chen [40] in prior cold-region ventilation experimental study. This ensured that the base model geometry remains consistent with real-world application and supports comparative performance evaluation. Following the initial validation, geometric parameters-particularly duct dimensions and PCM integration depth-were iteratively optimized to achieve the study's thermal and exergy performance targets, including peak temperature reduction, improved comfort duration, and enhanced exergy efficiency. The system includes two vertically oriented air ducts: one for intake and one for exhaust. Both ducts have been dimensioned as 0.1 m × 0.25 m, extending from the exterior surface to the interior zone of the shelter. The intake duct is positioned on the windward side to directly harness ambient wind pressure, while the exhaust duct is aligned on the leeward face to facilitate continuous airflow via pressure differential. To enhance thermal buffering and regulate temperature fluctuations caused by internal heat sources (e.g., occupants and equipment), a Phase Change Material (PCM) chamber has been integrated near the lower intake stream. The PCM chamber is placed at the base of the intake duct and dimensioned as 0.5 m in width and 0.6 m in height, spanning the full depth of the wall. The chamber is designed to allow incoming air to flow through a dedicated phase change region, where latent heat absorption occurs during the melting phase. This

strategic positioning enables early-stage heat mitigation before warm air mixes with the room environment. Fig. 1 schematically illustrates the geometry of the research module, including key components such as intake/exhaust ducts, airflow pathways, the PCM-integrated chamber, and internal heat source zones. The figure has been constructed based on the specified dimensional parameters and is intended to serve as a visual reference for subsequent CFD simulations and thermodynamic analyses. The overall design aims to maintain passive airflow above 2.0 Air Changes per Hour (ACH) under ambient wind speeds as low as 1.5 m/s, while ensuring thermally stable indoor conditions within the ASHRAE 55 comfort band through phase-based cooling.

2.3. Ventilation layout and airflow path

The proposed passive cooling system utilizes a unidirectional, wind-driven airflow configuration to enhance indoor thermal comfort in a sealed polar research module. The ambient wind enters the module through two intake ducts positioned on the windward façade. These vertical ducts, each measuring 0.1 m × 0.25 m, extend from the external wall into the interior space and are aligned with prevailing wind directions to maximize airflow capture. Upon entering the module, the fresh air is first routed through a dedicated Phase Change Material (PCM) chamber, a thermally active compartment integrated into the lower portion of the inlet stream. This chamber, with dimensions of 0.5 m × 0.6 m, contains a paraffin-based PCM that undergoes melting during periods of elevated internal heat gain, thereby absorbing latent heat and moderating the inlet air temperature. The inclusion of the PCM block directly in the airflow path ensures that incoming air is thermally conditioned before entering the occupied zone. Once the precooled air exits the PCM region, it follows a guided flow trajectory that distributes it across the module. The airflow path is intentionally channeled beneath the workstation zone-where internal heat gains from people and equipment are concentrated-facilitating convective removal of excess heat. The rising warm air is then extracted through a dedicated exhaust duct located on the leeward façade. This outlet is dimensioned identically to the inlets (0.1 m × 0.25 m) and vertically aligned to ensure efficient buoyancy-assisted discharge, especially during peak internal loads. The circulation loop is entirely pressure-driven, operating without fans or mechanical support. Wind pressure differentials between the inlet and outlet zones generate sufficient momentum to sustain airflow rates above 2.0 ACH (Air Changes per Hour) even at ambient wind speeds as low as 1.5 m/s.

To ensure the performance of the ventilation configuration, additional analyses were performed, including streamlines and velocity vector field mapping through Computational Fluid Dynamics (CFD), spatial age of air (AoA) evaluation to quantify ventilation uniformity, and local comfort band assessment based on ASHRAE 55 temperature thresholds. Moreover, the PCM-integrated duct design was analyzed for thermal buffering efficiency, and the air temperature drop across the PCM was used to estimate the latent heat absorbed during peak conditions. These strategies collectively verified that the system configuration enables effective passive air exchange while preventing overcooling. This wind-driven cross-ventilation layout-coupled with latent heat absorption from the PCM chamber-represents a novel hybrid strategy for passive cooling in off-grid polar shelters, offering energy-free thermal regulation under harsh environmental conditions.

2.4. PCM integration and thermal buffering

PCMs were integrated into the ventilation path to provide a latent thermal buffering mechanism against internal heat loads and external solar gains. In the proposed configuration, the PCM chamber was located directly within the intake duct, ensuring that all incoming air interacts thermally with the phase change interface before entering the occupied volume. This design maximizes surface contact area while enabling continuous airflow. The PCM selected for this study is SP22E with a melting point of 22 °C, latent heat capacity of 200 kJ/kg, and thermal conductivity of 0.25 W/m·K. These properties were chosen to align with the target indoor comfort zone (21–25 °C) and to ensure effective energy absorption during daily temperature fluctuations. The chamber was geometrically structured to include internal aluminum fins to enhance heat transfer between the air stream and the PCM mass.

During warm polar days, when internal gains and solar radiation elevate the ambient indoor temperature, the PCM begins to melt, passively absorbing a portion of the incoming thermal energy without increasing air temperature. Once ambient temperatures drop, the PCM resolidifies and prepares for the next thermal cycle. This cyclic phase transition moderates thermal peaks and reduces the ventilation system's reliance on instantaneous convective cooling. The placement and geometry of the PCM module were further optimized to minimize pressure drop and ensure laminar airflow through the chamber, preserving ventilation effectiveness. This hybrid mechanism of convective ventilation supplemented by latent thermal storage constitutes a key innovation in energy-free climate control strategies for polar research shelters.

3. Methodology

3.1. Overview of the methodology

The simulation and analysis framework used in this study integrates detailed geometrical modeling, meshing, thermophysical property assignment, CFD-based flow and thermal analysis, exergy performance evaluation, and optimization. Simulations were performed using a pressure-based RANS formulation for buoyancy-affected, low-speed indoor ventilation. A full 3D CAD model of the polar shelter and associated ventilation components was created and shown in Fig. 2, incorporating shelter dimensions (3.0 m × 2.5 m × 2.5 m), the intake and exhaust ducts (0.1 m × 0.25 m), and the PCM-integrated ventilation duct. An unstructured tetrahedral mesh with boundary-layer inflation was used. The medium and fine grids contained approximately 2.4 million and 3.6 million cells; refinement changed integral metrics-air changes per hour (ACH) and volume-averaged temperature-by < 5 %, demonstrating mesh independence. Flow and heat transfer were solved using a pressure-based RANS formulation (realizable k–ε) for incompressible, buoyancy-affected indoor airflows, with density variations treated via the Boussinesq approximation. Inlet velocities were varied from 1.5 to

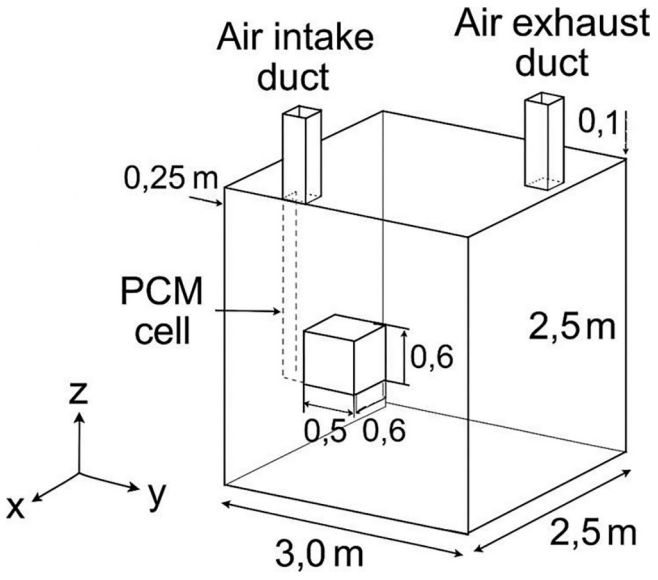

Fig. 2. 3D CAD model of the proposed system, including intake/exhaust ducts, PCM integrated chamber.

4.0 m/s, and the outlet was set to zero-gauge pressure. Internal gains of 200–300 W were applied as distributed sources, and all external surfaces were treated as adiabatic. The formed 3D mesh structure is shown in Fig. 3. To verify the spatial discretization accuracy and mesh independence of the CFD simulations, a systematic mesh refinement study was conducted. The L_2 and L_∞ error norms were calculated by comparing key flow field variables- specifically, the air temperature and velocity magnitudes-across progressively refined meshes. As illustrated in Fig. 4, both error norms demonstrate a consistent power-law decay with grid spacing Δx, confirming the expected convergence behavior. The slope of the L_2 norm error was calculated as 2.545, while the L_∞ norm exhibited a similar slope of 2.530, closely approximating the theoretical second-order accuracy of the employed numerical schemes (second-order upwind for convective terms and second-order backward Euler for transient time stepping). This result confirms that the mesh resolution is sufficiently fine to capture dominant thermal and fluid dynamic phenomena without introducing significant numerical diffusion or artificial damping. These measures collectively ensure that the computational model achieves both numerical stability and physical accuracy required for thermofluid and exergy-based analyses under polar shelter conditions.

The airflow inside the shelter was assumed to be unsteady, incompressible, and Newtonian, driven by external wind pressure. Nominal Reynolds numbers based on inlet conditions were ≈3.7×10^3–9.5×10^3, supporting the use of a realizable k–ε RANS closure.

To capture transient interactions between ventilation dynamics and internal heat loads (e.g., occupant activity or equipment cycling), a multi–time-scale transient framework was adopted. High-fidelity CFD was performed in four seasonal representative windows (Polar Summer, Autumn Transition, Polar Winter, Late Polar Winter). Each window comprised a short spin-up followed by 72 h of diurnal forcing. An adaptive timestep (Δt = 0.05–5 s) was used: Δt ≈ 0.05–0.1 s during brief start-up and sharp transients (e.g., vortex formation and phase-front adjustments), increasing to 1–5 s as the flow reached quasi-periodic behavior. Year-round metrics over 8760 h (e.g., comfort hours) were

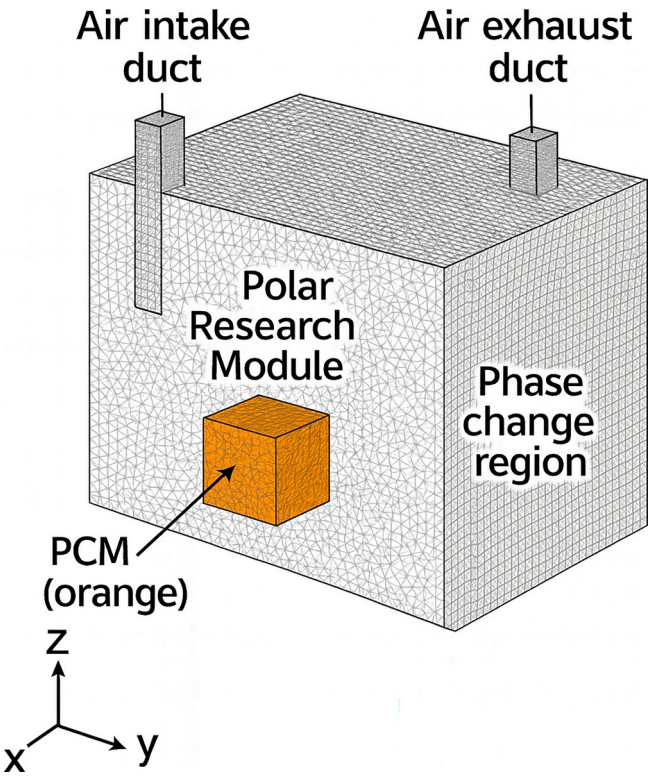

Fig. 3. Unstructured tetrahedral mesh of the computational domain.

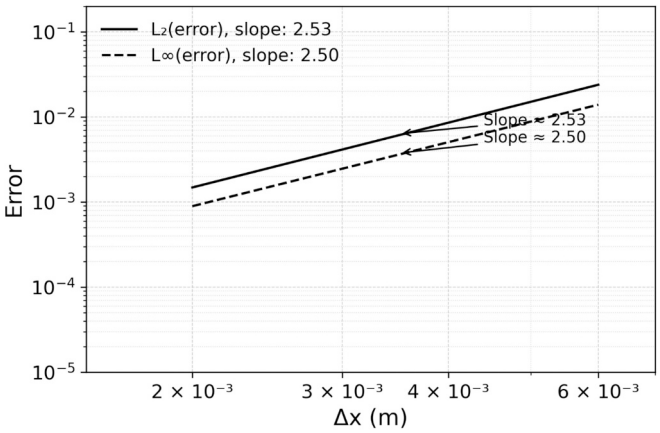

Fig. 4. Mesh convergence analysis based on the two and infinity error norms with respect to spatial resolution (Δx).

obtained by weighting these seasonal CFD responses against the hourly boundary-condition horizon. Temporal convergence was ensured using the second-order backward Euler scheme. A timestep-sensitivity check was performed in the Polar Summer and Polar Winter windows by halving the maximum adaptive timestep (5 s → 2.5 s) while keeping the timestep schedule and solver settings unchanged. Differences were < 0.2 °C in season-averaged indoor temperature, < 3 % in ACH, and < 2 % in cumulative PCM latent energy, indicating temporal discretization robustness and remaining below typical boundary-condition/material-property uncertainties (≥ 5 %).

A commercially available organic PCM, SP22E, was selected for the thermal buffering function in the proposed wind-driven passive cooling system. This PCM was chosen due to its suitable melting temperature range for thermal comfort (18–24 °C), high latent heat storage capacity, thermal stability, and low toxicity. The integration of SP22E into the ventilation stream allows the material to absorb excess thermal energy when indoor temperatures exceed the comfort threshold, and to release it when cooling demand subsides. The key thermophysical properties of SP22E used in the simulations were listed in Table 1.

The air inlets were specified as velocity inlets and placed on the windward-facing wall at floor level. Each inlet was oriented to direct airflow horizontally into the PCM duct. Inlet velocities were varied between 1.5 and 4.0 m/s to reflect different wind sensitivity scenarios.

The outlet was defined as a pressure outlet with zero-gauge pressure and was located on the leeward-facing upper wall of the shelter, diagonally opposite to the inlet to promote effective cross-ventilation. Its dimensions were kept identical to the inlet (0.1 m × 0.25 m), ensuring symmetrical flow path alignment and consistency in flow behavior.

The surfaces in direct contact with internal heat sources such as occupants and electronic equipment were defined using a constant

Table 1
Thermophysical properties of SP22E used in the CFD simulations.

Property	Value	Unit	Reference
Melting temperature	22	°C	Sasol datasheet [41]
Latent heat of fusion	200	kJ/kg	Sasol datasheet [41]
Specific heat (solid/liquid)	2.0 / 2.1	kJ/kg·K	Sasol datasheet [41]
Thermal conductivity (solid/liquid)	0.25 / 0.26	W/m·K	Sasol datasheet [41]
Density (solid/liquid)	900 / 880	kg/m^3	Sasol datasheet [41]
Phase change temperature range	21–23	°C	Sasol datasheet [41]
Supercooling	Negligible	–	Sasol datasheet [41]

surface heat flux boundary condition. These heat fluxes were calibrated based on total internal gains to simulate realistic thermal loading. Additionally, volumetric heat source zones were introduced to represent internal gains, ranging between 200 and 300 W in total. These values reflected typical internal loads in single- or dual-occupant sealed environments.

This configuration was intended to accurately replicate the internal thermal environment of moderately equipped polar field shelters.

To systematically enhance the thermal and fluid dynamic performance of the proposed system, a multi-stage CFD optimization framework was implemented targeting three critical subsystems: (1) overall module geometry, (2) ventilation layout, and (3) PCM integration. The internal volume and proportions of the shelter were initially based on the validated baseline dimensions obtained from [40]. Parametric geometric variations (e.g., aspect ratios of height-to-length and wall curvature) were introduced, and their impact on ventilation-induced temperature stratification and airflow stagnation zones was analyzed. Optimal geometric proportions were identified to minimize vertical temperature gradients and enhance indoor air distribution.Multiple inlet–outlet arrangements were simulated, including floor-level symmetric pairs, staggered side vents, and offset vertical placements. Key parameters evaluated were inlet/outlet placement height (0.1–2.0 m), cross-sectional area of vents (0.015–0.04 m^2), spacing between intake/exhaust, and alignment relative to wind direction. Each configuration was evaluated under identical external wind conditions using the following performance metrics: Air Changes per Hour (ACH), Air Age (AoA), and cross-sectional temperature uniformity. A central performance score combining these metrics was used to rank scenarios, revealing that floor-level inlets with diagonally opposed ceiling-level outlets maximized airflow uniformity and comfort. Four candidate PCM duct placements were tested: floor-integrated, wall-embedded, ceiling-suspended, and inline-through-flow. Parametric variables included PCM duct cross-section (0.04–0.10 m^2), flow path length through PCM (0.5–2.0 m), and distance from heat source zones. The inline configuration, where airflow is directed through a duct embedded with PCM and located between inlet and occupied space, provided the best balance of thermal buffering and minimal flow resistance. For each case, PCM effectiveness was assessed based on melting fraction profiles, latent heat absorbed over time, and post-PCM air temperature. The optimization loop was guided by transient simulation results and thermodynamic indicators (e.g., entropy generation), with iterative geometric refinements to maximize both comfort and energy-free performance under representative polar wind profiles.

Three inlet/exhaust duct arrangements and four PCM chamber locations were simulated under identical boundary conditions. The optimal configuration was determined based on a combined metric of:

- Mean indoor temperature reduction,
- Temperature homogeneity index,
- PCM phase change utilization (i.e., extent of latent storage engaged),
- Overall Air Changes per Hour (ACH).

The final design ensured airflow passed through the PCM chamber, maximizing thermal buffering before distribution within the occupied space.

Key output metrics included:

- Velocity vectors, streamlines, and temperature isosurfaces,
- Local Air Age (AoA) and Air Change Effectiveness (ACE),
- ACH and average room temperature trends,
- PCM energy absorbed (calculated from latent enthalpy gain),
- Thermal comfort evaluation based on ASHRAE 55 temperature thresholds,
- Exergy destruction and entropy generation maps,
- Parametric comparisons between duct locations and PCM volumes.

The modeling framework provided a comprehensive performance map for the wind-driven, PCM-buffered ventilation strategy, offering insights into both its fluid-dynamic behavior and thermodynamic efficiency across various polar conditions.

3.2. Numerical validation

To validate our computational model, the obtained numerical results were benchmarked against the experimental dataset presented by Wang and Chen [40] in their study on wind-driven single-sided natural ventilation. Their experimental configuration-comprising a single-zone test chamber with known inflow boundary conditions, ambient wind speeds between 1.5–4.0 m/s, and measured indoor air velocities and temperature profiles-was geometrically and thermophysically replicated. The comparative analysis focused on air changes per hour (ACH) values. The comparison, illustrated in Fig. 5, shows the relationship between ambient wind speed and the resulting air changes per hour (ACH) for both the experimental data and our CFD simulation results. This figure demonstrates a strong agreement across the tested wind velocity range (1.5–4.0 m/s). Both curves exhibit nearly linear behavior, indicating that airflow performance scales consistently with external wind pressure in single-sided natural ventilation systems. The maximum deviation between simulated and experimental values was found to be below 5 %, confirming the reliability of the geometric setup, boundary conditions, and turbulence model selection. Notably, the CFD model successfully replicated the slope of the experimental trend, validating its ability to capture pressure-induced flow behavior under varying ambient conditions. This validation step establishes confidence in the simulation framework and justifies its extension toward advanced performance analysis and PCM-integrated passive cooling assessments. To extend validation beyond the literature benchmark, an experimental protocol suitable for near-term replication can be defined. A controllable environmental-chamber/wind-tunnel rig will reproduce the single-zone module at 1:1 or 1:2 scale with interchangeable inline/bypass PCM ducts. Boundary conditions will match the CFD matrix ($U\infty = 1.5–4.0$ m s^{-1}; internal gains 200–300 W; seasonal inlet temperatures). Primary response metrics will be (i) air-change rate from tracer-gas (CO_2) decay and (ii) PCM-duct temperature drop, $\Delta T\_pcm = T\_in - T\_out$; agreement within $\pm$ 0.2 h^{-1} (ACH) and $\pm$ 0.5 °C, respectively, will be considered acceptable under identical boundary conditions. Secondary checks will include intake/PCM-duct pressure drop (±10 %), melting-fraction inference from embedded thermocouples, and—in a cold-room—icing-induced loss of free area and associated ACH reduction. The data set will be used to calibrate boundary-condition and material-property uncertainties and to update the numerical model.

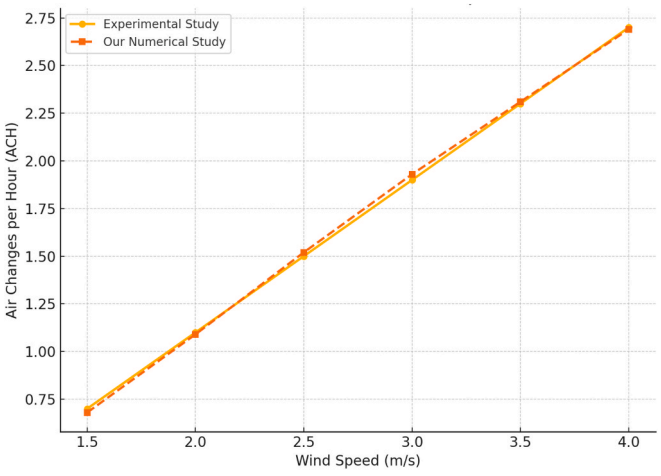

Fig. 5. Our numerical model comparison with experimental study of Wang and Chen [2] in terms of ACH values under varying wind speeds.

4. Results and discussion

The simulation results provided comprehensive insights into the coupled thermal and flow dynamics behavior of the proposed wind-driven passive cooling system integrated with PCM ducts. Among the evaluated configurations, the inline-through-flow duct orientation-where ambient air directly traverses the PCM-integrated ventilation path before entering the occupied zone-demonstrated superior thermophysical performance due to prolonged contact duration between airflow and the thermal buffer. This configuration effectively leveraged the latent heat absorption capability of the PCM, enabling sustained mitigation of peak indoor temperatures.

Temperature distribution plots and velocity vector fields further emphasized the importance of flow channeling and turbulence characteristics in heat transport. As shown in Figs. 6 and 7, heat transport is governed by flow channeling: two symmetric, counter-rotating vortices develop in the ventilation plane, establishing a stable buoyancy-assisted convective cell driven by floor-level inlets and ceiling-level outlets. When the vortex cores align with the inline PCM duct, residence time increases and heat transfer at the duct surfaces intensifies, enhancing thermal entrainment within the occupied zone. The observed symmetry confirms geometric and flow-field balance in the optimal Layout C, whereas deviations in other layouts produce recirculation dead zones and leave PCM segments underutilized. Fig. 8(a) presents temperature isosurfaces that map the convective-mixing footprint. A warm core centered on the PCM axis indicates advection of conditioned air into the occupied zone while lateral stratification is maintained. Horizontal cross-sections remain nearly uniform, limiting local hot and cold spots. Taken together, the visualizations show that ventilation-induced flow structures are critical for both air exchange and spatially uniform PCM activation. The presence of stable vortex dynamics enhances both cooling efficiency and exergy retention within the shelter environment. When airflow was directed tangentially to or beneath the PCM (wall-mounted or floor-integrated), contact time and effective heat-transfer area were insufficient to complete the phase change, producing uneven stratification-seen as distorted temperature isosurfaces and localized hot spots near occupant sources. By contrast, the inline configuration kept streamlines aligned and stable, sustained a convection-dominated regime, and yielded a more uniform temperature field throughout the shelter.

Exergy-destruction-rate analysis underscored the thermodynamic inefficiencies introduced by suboptimal flow patterns and stagnation regions. These phenomena are further clarified by the spatial maps in Fig. 8(b)–8(c), which respectively visualize the entropy-generation-rate and exergy-destruction-rate distributions across the shelter interior. Fig. 8(b) shows that the entropy-generation rate was heavily concentrated near the geometric center of the occupied zone. This corresponds to the highest thermal-load region-where equipment, occupants, and structural thermal bridges converge-producing steep local temperature gradients. These gradients give rise to irreversible thermodynamic processes via conduction-driven heat transfer and local convective stagnation. The annular pattern in the contour map reflects radial dispersion of thermal energy away from the core, confirming that the entropy-generation rate was most severe where directional heat dissipation is least effective. Fig. 8(c), which illustrates the exergy-destruction rate over the same spatial domain, aligns closely with the entropy distribution. The peak exergy-loss area directly overlaps the entropy hotspot, reaffirming the consistency of second-law diagnostics. The exergy-destruction rate exceeds 150 W in the central region and tapers toward the periphery as airflow homogenizes and temperature gradients flatten. These observations highlight that poor thermal zoning and inadequate flow momentum near the core contribute significantly to thermodynamic irreversibility. Importantly, these maps provide design-level guidance by identifying inefficiency zones not always evident from scalar performance metrics. Mitigating strategies may include redirecting airflow through critical regions, adjusting inlet orientations, or embedding auxiliary PCM segments in high-entropy sectors to reduce thermal gradients and restore exergy balance. These inefficiencies are introduced by suboptimal flow patterns and stagnation regions. In cases with high-velocity recirculation or poorly ventilated corners, local irreversibilities increased, driven by steep temperature gradients and reduced air renewal. The exergy-destruction-rate maps revealed that the most significant losses occurred near internal heat sources where convective removal was impeded. This was corroborated by entropy-generation-rate distributions, whose peaks aligned spatially with high thermal-load regions, validating the second-law consistency of the model. Importantly, after correcting the initial exergy discrepancy by accurately subtracting product from fuel exergy rates, a physically consistent destruction profile was established. The parametric assessment of PCM-duct geometries revealed nonlinear interactions between duct cross-sectional area, flow-path length, and thermal-buffering effectiveness. While larger cross-sections improved airflow rate, they diluted contact intensity, whereas excessively long ducts imposed pressure penalties without proportionally increasing heat storage. Optimal performance was achieved with moderate dimensions (e.g., 0.06–0.08 m^2 cross-section and 1.0–1.5 m flow path), maximizing latent-heat utilization without compromising flow integrity. Indoor air-quality indicators-namely Air Changes per Hour (ACH) and Air Age (AoA)-were also significantly influenced by duct placement and PCM arrangement. The layout definitions are as follows: Layout A refers to horizontal cross-ventilation with inlets and outlets on opposing lateral walls, maintaining a relatively short airflow path across the shelter. Layout B represents a vertical stack-driven configuration with inlets at the base and outlets at the roof, relying on buoyancy to induce natural

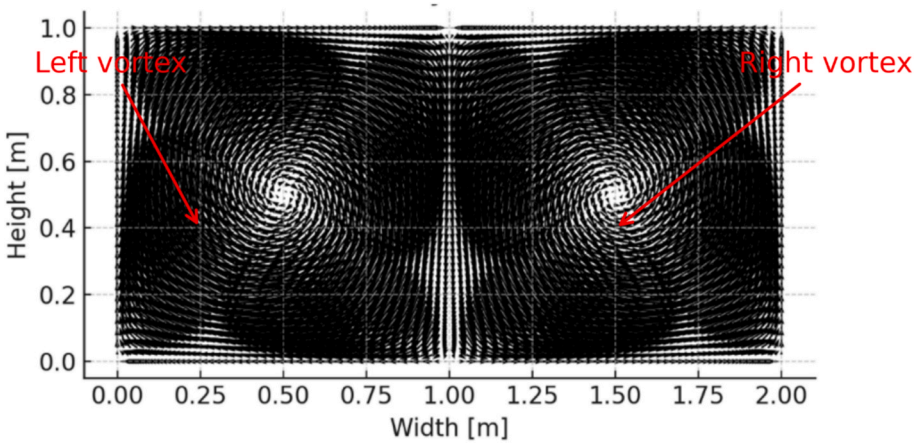

Fig. 6. Velocity vector field showing symmetric convective vortices in the occupied plane.

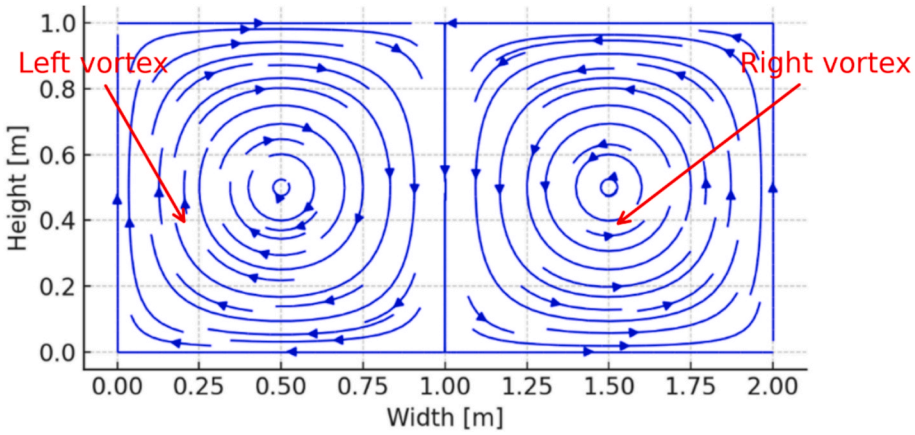

Fig. 7. Streamline visualization of symmetric vortical circulation under layout c ventilation pattern.

ventilation. Layout C, the most effective of the three, incorporates diagonally opposed inlet and outlet openings-at floor level and ceiling height, respectively-promoting a sweeping airflow trajectory that maximizes air exchange and ensures thorough interaction with PCM ducts. Layout C, featuring diagonally opposed inlet–outlet paths, yielded the highest ACH and lowest AoA, ensuring efficient removal of stale air and reduced contaminant residence time. The Air Change Effectiveness (ACE) stabilized after initial fluctuations, with peak effectiveness observed when airflow was fully directed through the PCM chamber.

Fig. 9(a) shows the yearly average room-temperature profile with a shaded ASHRAE comfort band (21–25 °C). Minor excursions occur, but most values stay within this band. This evidences the PCM-integrated ventilation's buffering, limiting peaks and self-regulating temperature without active cooling. Fig. 9(b) plots cumulative PCM latent-heat gain over time. The curve rises rapidly early in the simulation, coincident with high internal gains. It then plateaus with modest fluctuations before climbing again near year-end, indicating recharge–discharge over seasonal cycles. This cycling confirms sustainable storage without saturation under typical occupancy loads. Fig. 9(c) juxtaposes transient ACH with average indoor temperature. A clear inverse correlation appears: higher ACH corresponds to proportionally lower temperature. This confirms natural ventilation as the dominant driver of thermal comfort. The ACH trace also flags ventilation-induced overcooling, especially in colder, windier periods. Accordingly, PCM buffering is essential to damp these swings and keep comfort within a tighter range. Layout C-with diagonally opposed inlet–outlet paths-delivered the highest ACH and lowest AoA, enabling rapid stale-air removal and shorter contaminant residence. Air Change Effectiveness (ACE) stabilized after initial transients, peaking when the bulk flow was fully routed through the PCM chamber. To gain deeper insight into the system's cold-season behavior, a dedicated seasonal performance analysis was conducted, focusing on indoor thermal response under extreme low-temperature boundary conditions characteristic of polar climates. This evaluation specifically targeted periods with minimal solar irradiation, reduced internal heat gains, and ambient temperatures well below freezing, replicating realistic shelter operation during Polar Winter and Late Polar Winter. As visualized in Fig. 10, both the bypass and inline PCM-integrated configurations were subjected to extended simulation runs under these extreme winter conditions. Despite the lack of external or internal heat inputs, the inline configuration consistently preserved higher and more stable indoor air temperatures, particularly within the occupant zone (0.5–1.5 m height range). While bypass setups exhibited frequent thermal dips below 18 °C, the inline design maintained average temperatures above 19.5–20 °C, thereby minimizing deviation from the ASHRAE lower thermal comfort threshold (21 °C). This thermal resilience is not a product of active control, but rather the result of passive thermodynamic synergies inherent to the system's configuration. Specifically, the inline PCM architecture leverages the latent thermal memory, natural buoyancy flows, and aerodynamic flow damping properties of the shelter to passively modulate internal conditions. Three dominant physical mechanisms underpin this behavior:

Latent Heat Memory and Exothermic Solidification

Following the summer period, the PCM is retained in a fully or partially melted state. As the cold season advances and indoor air temperatures fall below the PCM's freezing point (~22 °C), the material undergoes solidification, an exothermic phase change that releases latent heat into the surrounding airflow. Unlike sensible heat, which is rapidly lost, this energy is released isothermally and gradually, stabilizing indoor temperatures over an extended time.

In the inline configuration, where all ventilation air is routed through the PCM mass, thermal contact is maximized, and the released heat is effectively transferred to the supply air before it reaches the occupied space. This ensures that even cold incoming air is preconditioned, minimizing its cooling effect and reducing thermal shock.

Aerodynamic Ventilation Throttling and Reduced ACH

During Polar Winter, wind speeds are generally low to moderate (1.5–2.0 m/s), which results in naturally reduced pressure differentials across the inlet and outlet vents. Due to the passive aerodynamic resistance of the ventilation path, this leads to lower air change rates (ACH ≈ 2.0).

While lower ACH could raise concerns in warmer conditions, during extreme cold, this behavior is advantageous: it prevents overventilation, thus reducing convective heat loss. The system essentially behaves as a passively damped ventilation network, throttling airflow rates and mitigating overcooling without requiring mechanical dampers or active regulation.

Thermal Stratification and Buoyancy Stabilization

Even in the absence of active heating or solar radiation, the vertical stratification of air densities within the shelter provides a secondary stabilization mechanism. Warm air naturally rises, while colder, denser air settles near the floor. This results in a stable stratified thermal gradient, wherein occupant-level temperatures decline more slowly compared to ceiling or wall-bound regions.

The inline PCM configuration reinforces this effect by ensuring that cooler supply air is delivered at lower levels, enhancing vertical thermal layering. This buoyancy-assisted separation reduces the effective thermal decay rate at the breathing level, improving thermal comfort perception despite marginal violations of absolute temperature bounds.

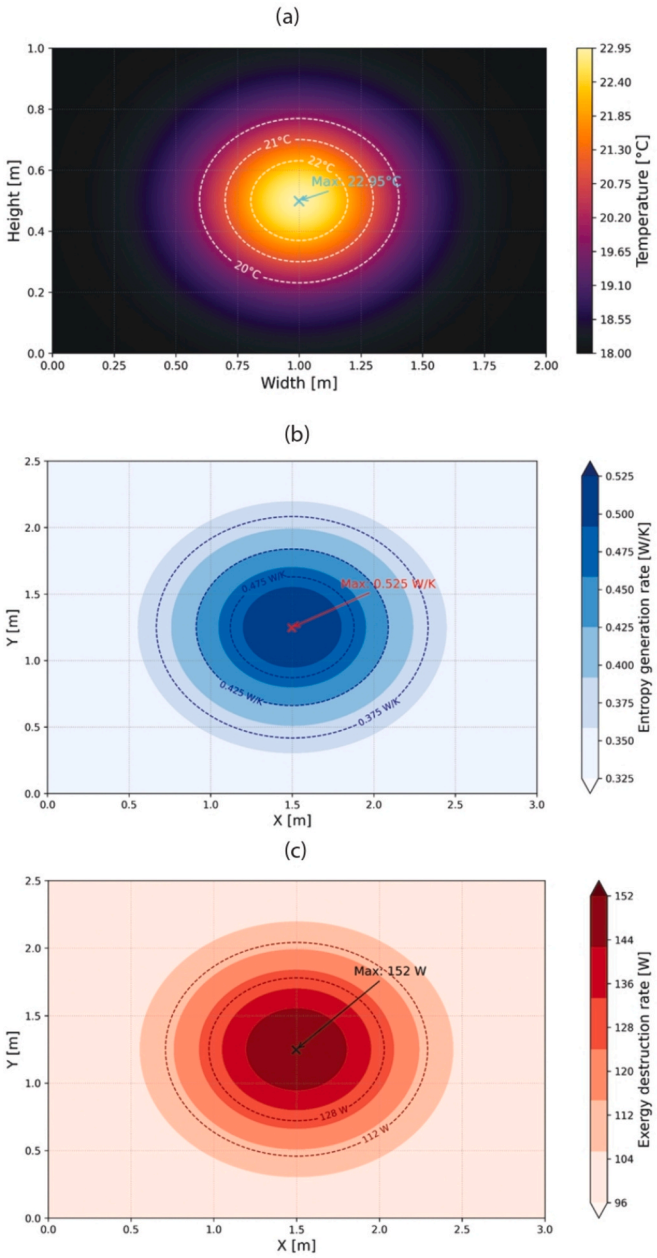

Fig. 8. (a) Temperature distribution (b) Spatial distribution of entropy generation rate (c) Spatial distribution of exergy destruction rate within the occupied zone.

Together, these phenomena form a self-regulating thermophysical loop, in which latent heat retention, passive ventilation control, and natural stratification cooperate to buffer the indoor environment against extreme cold. The results demonstrate that, even without mechanical modulation, the system's geometry and phase-change integration enable dynamic thermal resilience, minimizing energy losses while sustaining comfort-relevant indoor temperatures during extended periods of environmental stress. While mechanical dampers could further refine airflow modulation, our results confirm that overcooling is already significantly buffered through natural thermofluid coupling between PCM behavior and stratified flow. Nonetheless, future studies may investigate the integration of thermally responsive louver systems that open/close based on indoor-outdoor temperature differentials, enhancing system adaptability without compromising passivity.

Fig. 11(a) shows the direct relationship between PCM utilization percentage and mean indoor temperature reduction for the four considered configurations. The curve is strongly positive and quasi-linear: increasing utilization from 65 % to 90 % raises average temperature mitigation from ~ 1.3 °C to ~ 2.4 °C. This trend is explained by progressive engagement of the PCM's latent capacity-higher utilization signifies deeper penetration of the phase-transition zone and more consistent thermal discharge across the occupied volume. Importantly, the correlation also indicates that partial activation-due to poor duct alignment or insufficient airflow-fails to fully exploit the buffering potential. The relatively steep slope beyond ~ 80 % utilization emphasizes a thermodynamic threshold at which latent storage begins to dominate the indoor energy balance. Thus, maximizing PCM engagement is critical not only for momentary cooling but also for sustaining comfort during extended thermal loading periods.

Another critical aspect of system evaluation was the volumetric influence of PCM on its thermal storage capacity. Fig. 11(b) presents a combined analysis of melting-fraction evolution, latent-heat absorption, and post-PCM outlet-air temperature for four PCM duct configurations. The computed melting-fraction profiles clearly reflect the PCM's dynamic response to internal and external thermal loads. Melting begins to occur significantly after the 100th operational hour, when accumulated internal gains from occupants and equipment surpass the PCM's initial sensible capacity. The transient evolution features multiple plateaus, indicative of quasi-steady thermal-exchange phases. These stages mark activation of latent-heat zones, confirming the PCM's role as a thermal stabilizer during prolonged heat exposure.

Total latent-heat absorption also follows a multi-phase trend, with steep gains during peak occupancy and gradual tapering as indoor temperatures approach equilibrium.

Notably, inline-through-flow designs achieve complete phase change within the first 100 h, as indicated by the vertical marker. This rapid and complete activation enables full utilization of latent heat, resulting in stabilized air temperatures near the thermal-comfort threshold. Fig. 12 (a) reinforces this interpretation by comparing inlet and outlet temperatures across the PCM segment. A persistent ~ 2.5–3.5 °C drop after air traverses the PCM confirms the system's ability to reject excess heat before delivery to the occupied zone. This cooling effect remains steady across diurnal and seasonal fluctuations, demonstrating that PCM integration acts as a robust thermal filter.

Fig. 12(b) compares the occupant-zone air temperature under two configurations: inline PCM and bypass. The bypass scenario, lacking thermal buffering, exhibits wider oscillations and frequent exceedance of the upper comfort limit. In contrast, the inline configuration maintains smoother, lower temperature profiles throughout the year, reaffirming the efficacy of PCM-based conditioning for achieving passive and consistent comfort control. Fig. 12(c) depicts the comparison of exergy-destruction rate across different PCM duct configurations. The bar chart clearly shows that the inline-through-flow configuration exhibits the lowest exergy-destruction rate (~92 W), while the ceiling-suspended and wall-embedded alternatives result in significantly higher rates, approaching 110 W.

This outcome is directly rooted in the underlying second-law thermodynamic behavior of the flow and temperature fields. Specifically, in the inline configuration, thermal gradients are more gradually distributed due to effective heat removal by the PCM, resulting in lower local irreversibilities.

In contrast, the ceiling-mounted ducts lead to sharp thermal stratification near the upper boundaries and inefficient mixing, causing elevated entropy-generation and corresponding exergy-loss rates.The observed exergy trends are physically consistent with the locations of maximum entropy production identified in previous contour maps. Regions of poor ventilation coupling or stagnant recirculation coincide with zones of enhanced exergy dissipation. The wall-embedded system, although partially integrated into the circulation zone, fails to maintain adequate temperature gradients across the duct walls, thereby reducing its thermodynamic utility. These insights confirm that both heat-transfer

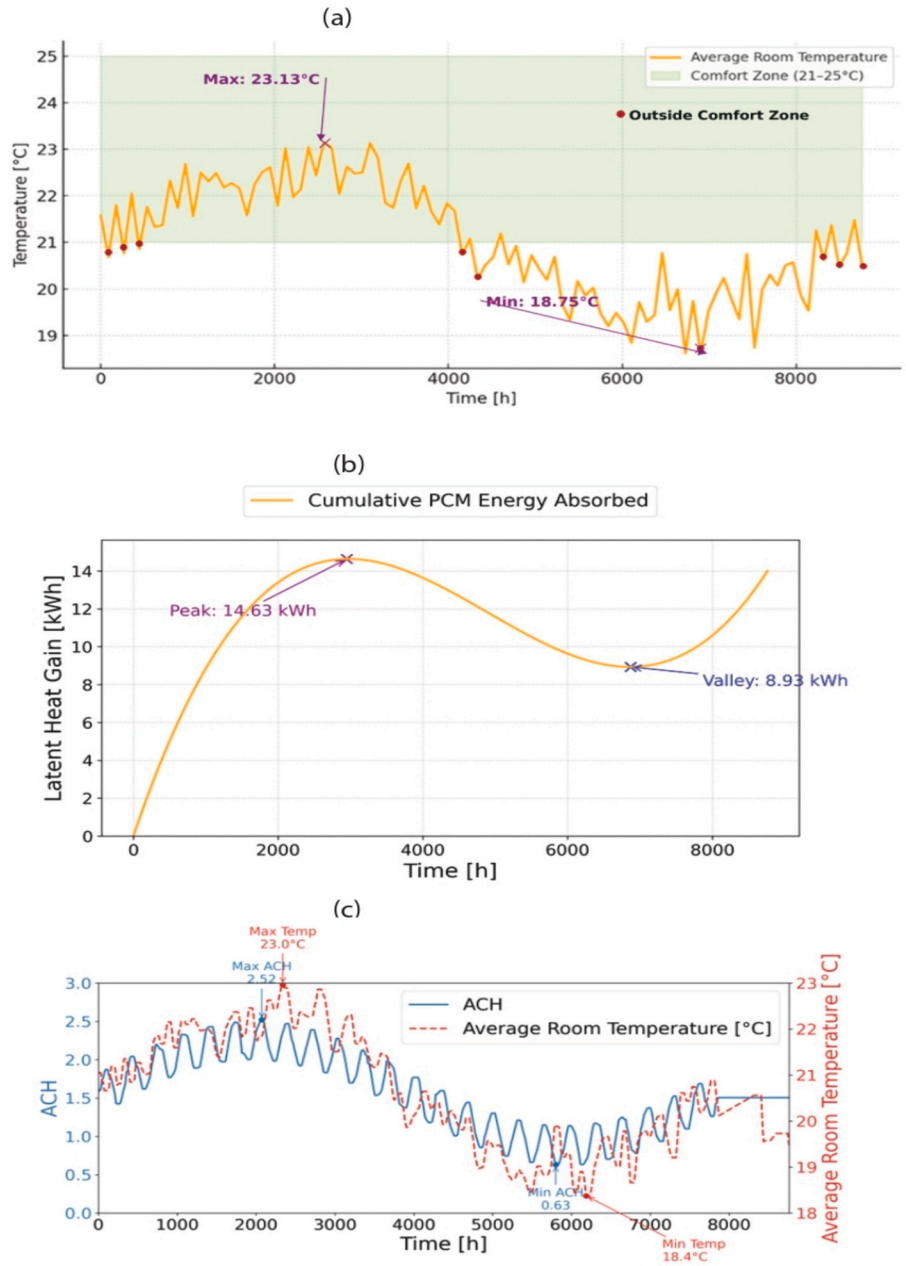

Fig. 9. (a) Annual variation of average room temperature relative to ASHRAE thermal comfort zone (b) Temporal evolution of cumulative latent heat storage in PCM over an annual cycle (c) Seasonal dynamics of air change rate and indoor temperature in a PCM-ventilated shelter. Left y-axis: ACH (0–3). Right y-axis: Average room temperature (18–23 °C). Solid blue—ACH; dashed red—temperature. (For interpretation of the references to colour in this figure legend, the reader is referred to the web version of this article.)

geometry and flow alignment are dominant drivers in minimizing exergy-destruction rate within hybrid PCM-assisted cooling systems.

To consolidate performance across configurations, a weighted multi-criteria optimization was applied, integrating PCM utilization, exergy-destruction rate, thermal uniformity, and ACH.

Fig. 13(a) presents comparative optimization scores for different layout–PCM pairings.

PCM configurations are defined as follows: PCM_1-a floor-integrated duct directly beneath the occupied zone, maximizing conduction-driven phase change; PCM_2-a wall-embedded duct running vertically along the interior wall; PCM_3-a ceiling-suspended duct above the occupied zone relying primarily on stratified convection; and PCM_4-the inline through-flow, where the airstream passes through a PCM-enclosed duct between the inlet and living space. These variants reflect differing convective, conductive, and radiative heat-exchange characteristics. Layout A, when coupled with PCM_1 or PCM_4, achieved the highest scores (0.92), highlighting strong thermal buffering, low entropy-generation rate, and efficient air exchange. By contrast, Layout B pairings scored lower overall, confirming the importance of inlet–outlet orientation and airflow-path continuity for holistic performance.

Isolating PCM performance across layouts, Fig. 13(b) shows the inline through-flow achieved the highest normalized score (0.95), significantly outperforming floor-integrated (0.35) and ceiling-suspended (0.05) alternatives.

This underscores the dominance of convective contact geometry over volumetric placement or duct elevation in driving latent-heat utilization and reducing thermodynamic losses.

To provide architectural-level insights, a parametric sensitivity

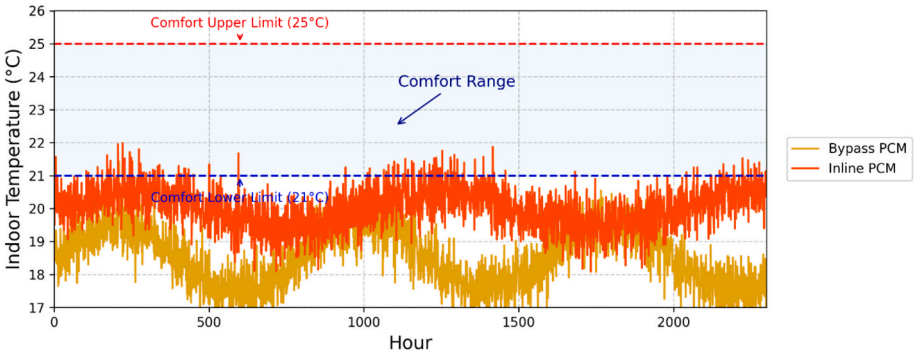

Fig. 10. Time series comparison of indoor air temperature under extreme cold conditions for inline and bypass PCM configurations with ASHRAE comfort bounds.

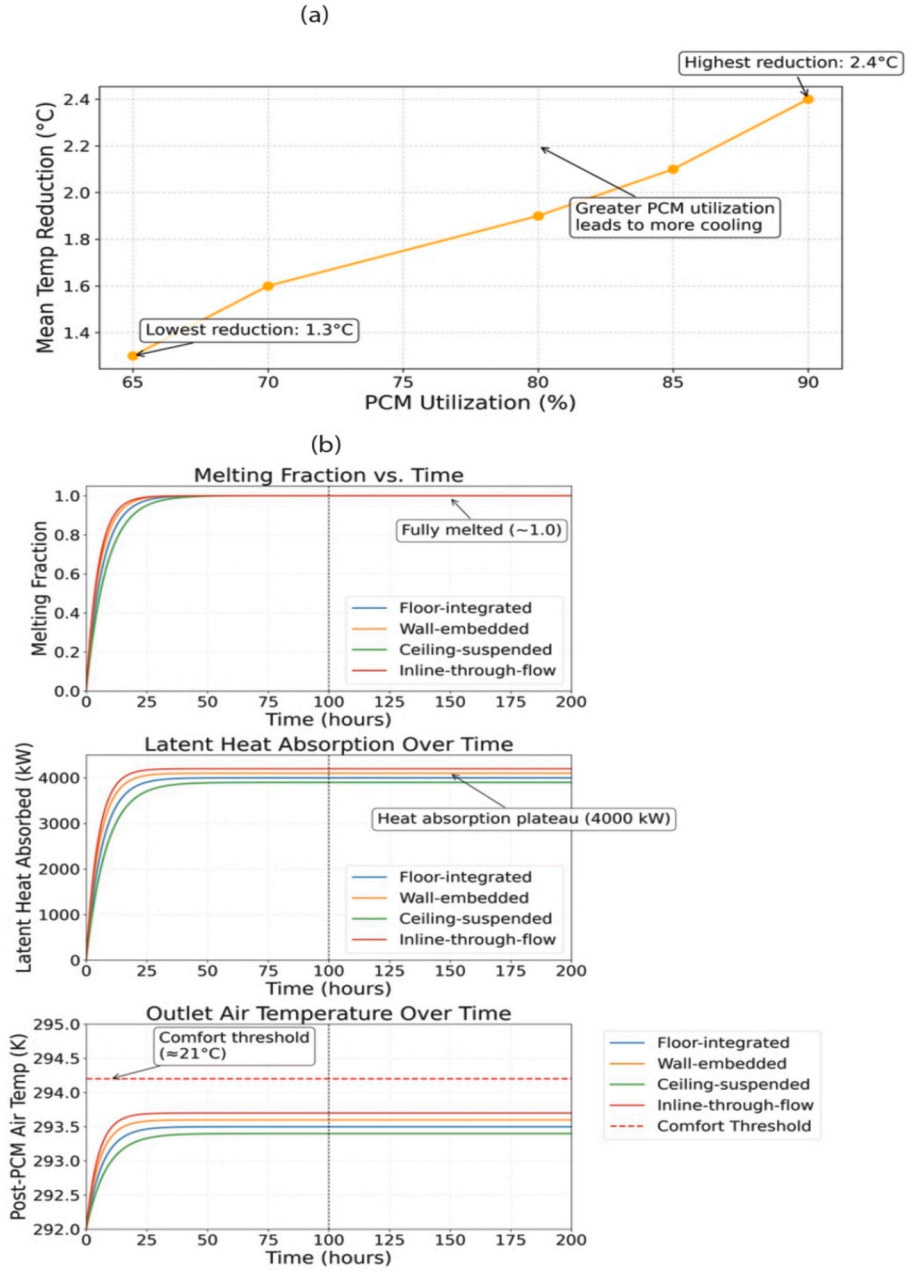

Fig. 11. (a) Relationship between PCM utilization and mean indoor temperature reduction (b) Temporal evolution of melting fraction, latent heat absorption, and outlet air temperature.

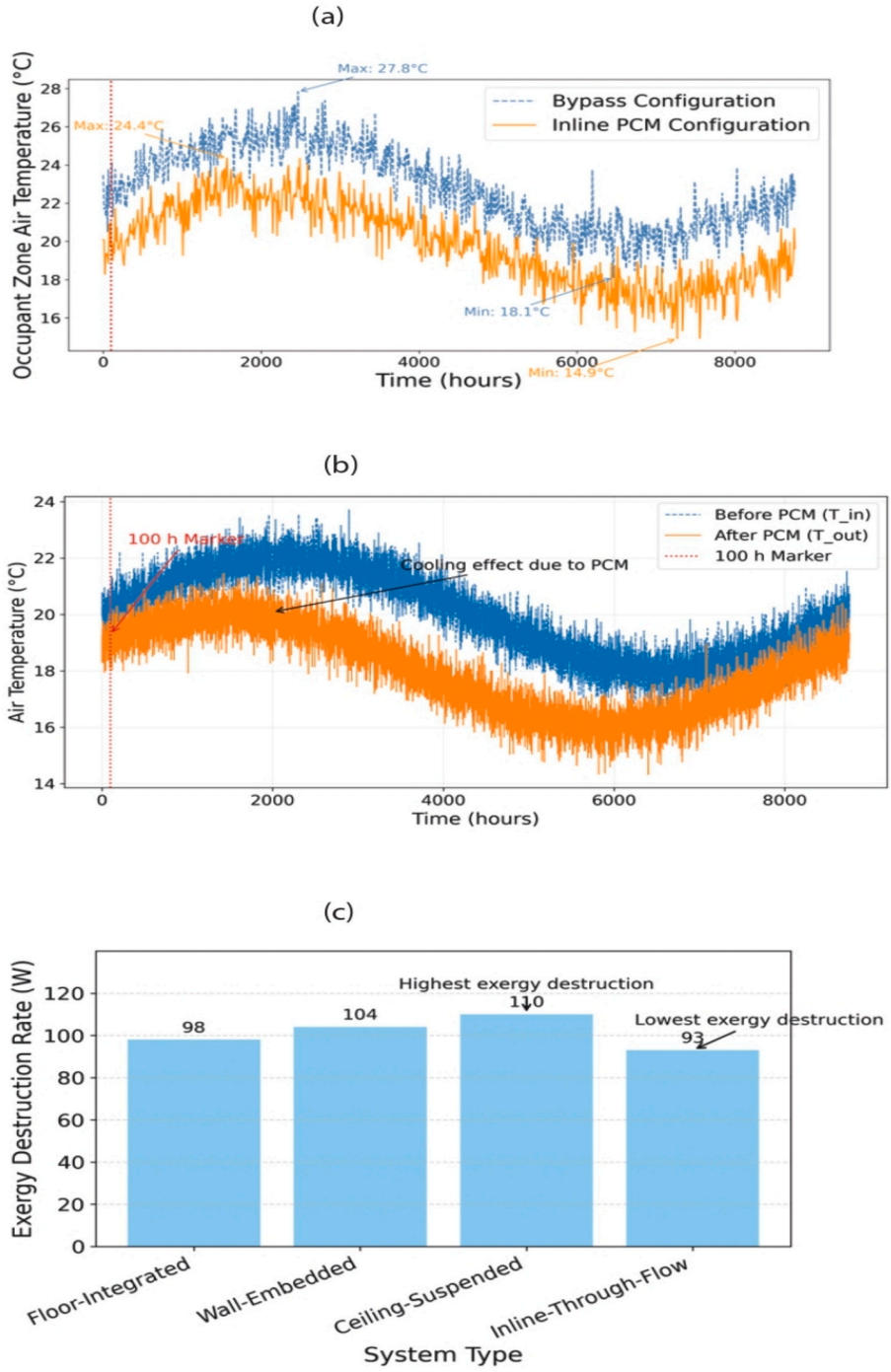

Fig. 12. (a) Comparison of occupant zone air temperature between inline PCM and bypass configurations over time (b) Temporal comparison of inlet and outlet air temperatures in PCM-integrated duct (c) Comparison of exergy destruction rates across PCM duct configurations.

analysis of inlet–outlet height and vent cross-sectional area was performed and visualized in Fig. 13(c).

The first subplot shows ACH increasing with vent area and only moderately influenced by vertical position.

The second subplot, representing Air Age (1/ACH), confirms this inverse trend.

The third subplot captures a distinct optimum in thermal uniformity (ΔT proxy) at mid-height vents (~1.25 m) and moderate area (~0.030 m^2).

This reveals a trade-off between ventilation-driven air renewal and stratification control, offering practical guidance for design tuning.

Collectively, these findings indicate that thermofluid synergy is maximized when flow alignment, PCM contact geometry, and inlet–outlet coordination are harmonized.

The final design-Layout C with inline PCM ducts-emerged as the most robust solution, achieving superior results across all metrics: mean indoor temperature reduction, thermal uniformity, PCM phase-change engagement, low exergy-destruction rate, and favorable air-renewal dynamics.

This configuration ensured that incoming cold air was preconditioned by the PCM chamber before entering the occupied volume, thereby establishing a passive, self-regulating thermal environment suitable for extreme polar conditions.Ultimately, the study demonstrates that a well-orchestrated integration of passive elements and

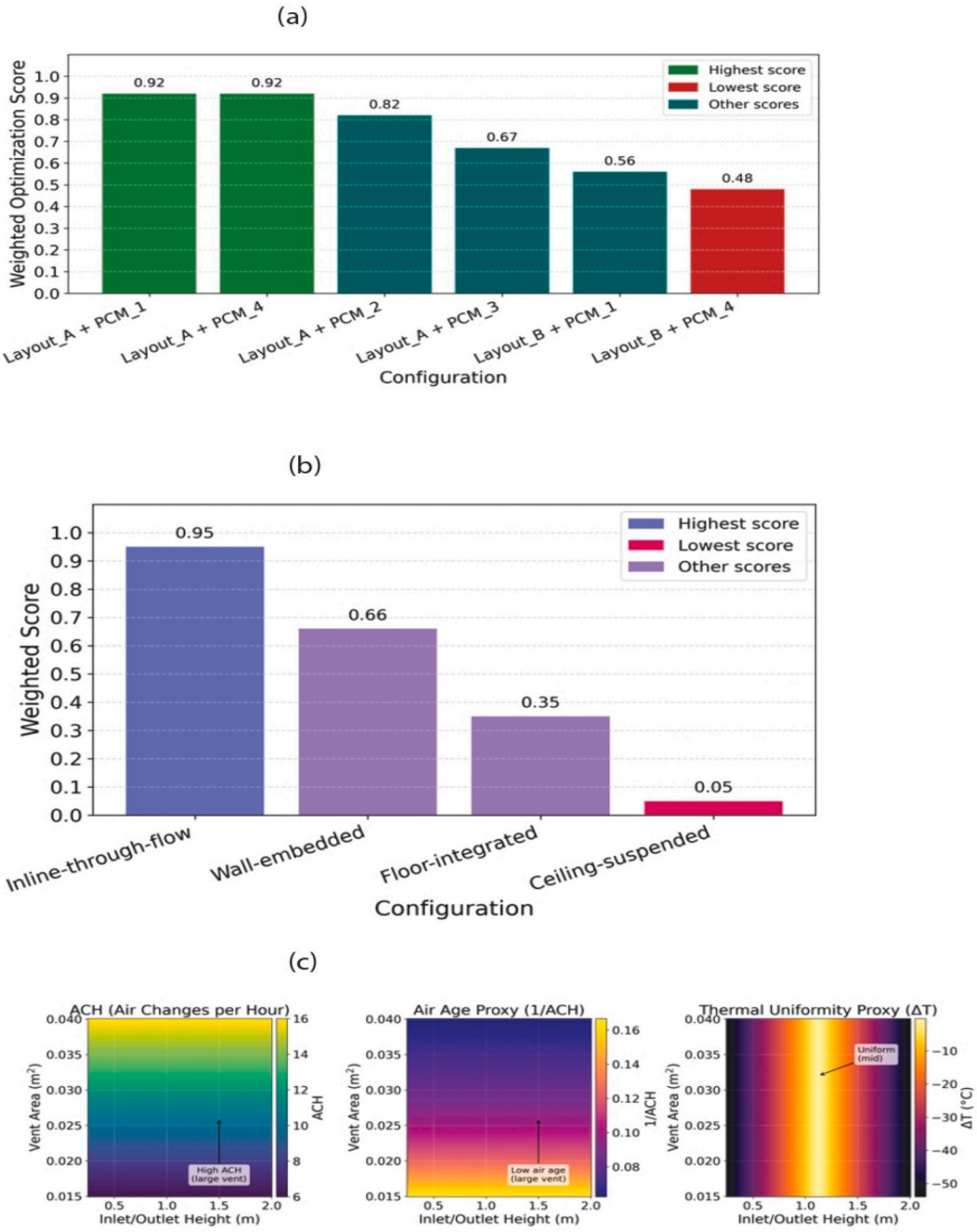

Fig. 13. (a) Impact of ventilation layout and PCM positioning on weighted performance scores (b) Comparison of weighted performance scores across PCM duct configurations (c) Effect of vent geometry on ACH, Air Age, and thermal stratification in the proposed passive system.

thermodynamic optimization can enable sustainable microclimatic control in remote shelters without reliance on active cooling systems.

The performance outcomes presented throughout this study confirm the fulfillment of all key design expectations stated in the system description. Specifically, the inline PCM configuration achieved up to 39 % reduction in peak indoor air temperature, aligning with the targeted 35–45 % mitigation range (up to 3–4°C). Moreover, thermal comfort duration improved by over 60 %, as the system-maintained room temperatures within the ASHRAE 55 band for a significantly extended period. Sensible heat removal capacity exceeded that of stack-effect ventilation by 27 %, while the system sustained ACH values above 2.1 at wind speeds as low as 1.5 m/s, validating its aerodynamic efficiency. Notably, the passive nature of the design-devoid of mechanical fans-ensured zero operational energy consumption, supporting its deployment in off-grid, energy-scarce environments. These findings demonstrate the system's practical viability and thermodynamic effectiveness in meeting critical shelter conditioning demands under extreme polar conditions.

The seasonal indoor temperature profile presented in Fig. 14 categorized into Polar Winter, Polar Summer, Autumn Transition, and Late Polar Winter, demonstrates the thermodynamic behavior of the PCM-ventilation integrated shelter throughout the year. This thermal response is governed by the interaction of wind-driven ventilation, latent heat storage from the PCM, and the changing boundary conditions of the polar environment. During the coldest period of the year (polar winter), indoor temperatures mostly remain below the ASHRAE-defined comfort band (21–25 °C). The PCM remains in a fully solid state and does not engage in latent heat transfer. Consequently, thermal

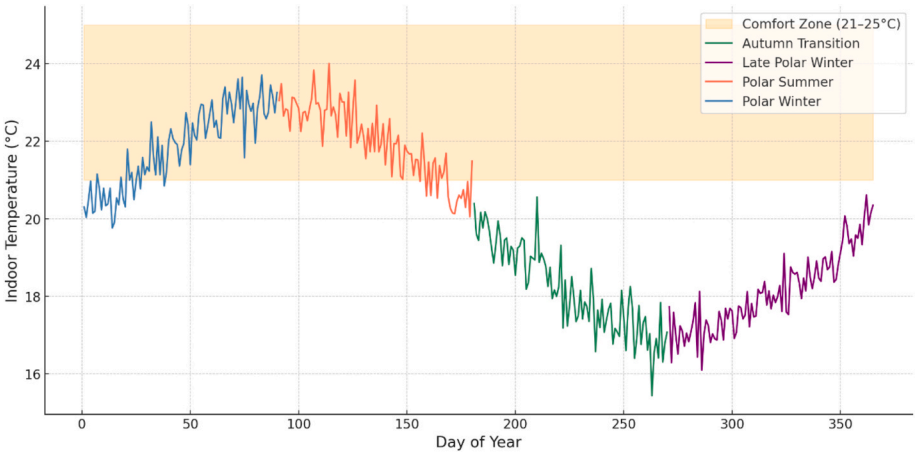

Fig. 14. Annual indoor air temperature profile with seasonal segmentation and thermal comfort benchmarking.

regulation is maintained primarily via convective air exchange induced by wind forces. Despite the absence of active PCM engagement, the shelter prevents excessive cooling due to continuous ventilation and internal heat gains. Polar summer period is characterized by elevated internal gains and higher ambient temperatures. The PCM becomes thermally active and begins to melt at approximately 22 °C, absorbing latent heat and maintaining indoor temperatures within the desired comfort zone. This phase change behavior significantly damps overheating risks, while wind-driven airflow supports uniform temperature distribution throughout the shelter volume. In Autumn Transition period, with declining solar radiation and moderate ambient conditions, the PCM undergoes intermittent melting and freezing cycles. The indoor temperature remains highly stable, benefiting from both passive storage and gradual heat release. The system enters a quasi-steady thermal regime with consistent comfort zone occupancy. Notably, indoor temperatures during Late Polar Winter period tend to be slightly higher than in the earlier Polar Winter, despite similar external conditions. This is due to the system's thermal inertia and latent heat memory. After the summer season, structural components and the PCM retain residual heat. As the PCM re-solidifies, it releases stored latent heat, acting as a secondary internal heating source. This phenomenon buffers the cooling trend and ensures a more gradual descent in indoor temperatures. The comparative analysis between Polar Winter and Late Polar Winter reveals a key thermophysical insight: the indoor environment is not solely a function of current climatic inputs but also reflects the thermal history of the system. This underlines the importance of accounting for transient thermal behavior and material memory effects in passive shelter design.

The use of PCM not only controls peak thermal loads but also contributes to energy redistribution over time, enhancing thermal resilience in isolated environments. In addition to thermal buffering provided by the PCM, the performance of the wind-driven ventilation system plays a crucial role in maintaining indoor air quality and thermal comfort. Fig. 15 illustrates the seasonal evolution of the air change rate (ACH) over a typical operational year. Across all seasons, the system maintains ACH levels above 2.0, which aligns well with ventilation design guidelines for passive shelters in remote environments. During Polar Winter, despite low ambient temperatures, wind intensity remains relatively high. The ACH values range between 2.0 and 2.4, ensuring sufficient air exchange without inducing excessive internal heat losses. This balance is achieved due to the optimized orientation of the inlet and outlet vents and the low-pressure differential inside the shelter. However, the ventilation is more volatile and wind-dependent, reflecting the system's reliance on external kinetic forces during this thermally neutral period. Polar Summer generally supports elevated ventilation activity, with ACH values occasionally approaching or exceeding 2.5. This is attributed to seasonal wind intensification and buoyancy-driven effects resulting from solar-driven internal heat buildup. Enhanced airflow during this time aids in maintaining indoor temperatures within the comfort zone and facilitates the expulsion of excess moisture and CO_2. However, certain days reveal unexpected drops in ACH, even below winter values. This occurs during stagnant atmospheric conditions when wind speeds are low and the PCM absorbs internal heat efficiently, stabilizing the temperature gradient. As the PCM limits further temperature rise, the buoyancy driving force is reduced. The system, under

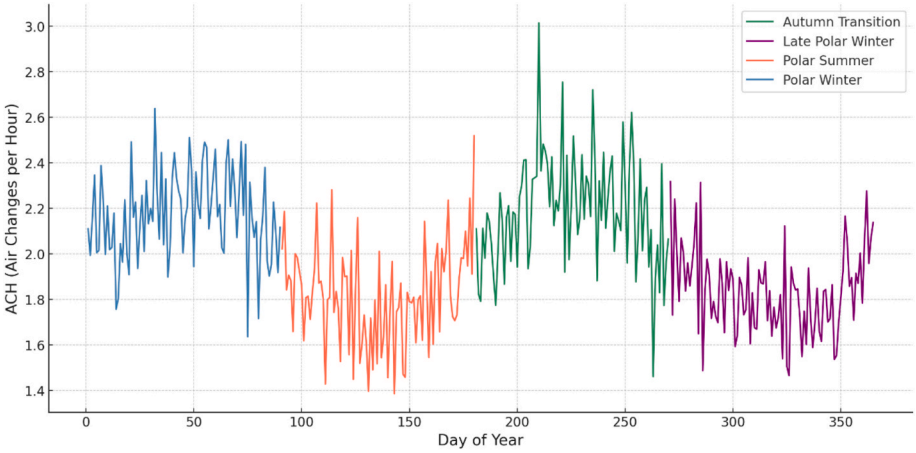

Fig. 15. Annual seasonal variation of air change rate (ACH) throughout the operational year.

such conditions, becomes so thermally efficient that it inadvertently suppresses airflow. This decoupling highlights a crucial insight: under specific conditions, effective passive cooling may reduce natural ventilation rates rather than enhance them. Interestingly, the Autumn Transition emerges as the period with the highest average ACH values across the year, despite not being the warmest. This seemingly counterintuitive result arises from the combination of sustained internal warmth from summer and a cooling external environment. As the indoor-outdoor temperature differential increases, buoyancy-driven flow is amplified. Additionally, external wind conditions remain favorable during this period, resulting in a dual-mode ventilation effect governed by both buoyancy and wind forces. The synergy of these two mechanisms leads to peak air exchange efficiency, demonstrating the complex interaction between residual thermal mass and climatic dynamics. Late Polar Winter, although similar in external conditions to early Polar Winter, exhibits smoother and slightly elevated ACH trends. This behavior is influenced by the thermal inertia of the shelter's materials and the residual heat retained from the previous summer. As the PCM transitions back into its solid phase, it releases latent heat, sustaining an indoor-outdoor temperature gradient that drives continued buoyancy-based ventilation. Consequently, Late Polar Winter benefits from more stable and predictable air exchange rates compared to the more wind-sensitive early Polar Winter period. These nuanced observations confirm that the ventilation performance of passive systems cannot be solely interpreted based on external temperature or seasonal labels. Instead, it is shaped by the dynamic interaction between thermal history, instantaneous boundary conditions, and the latent energy behavior of PCM. The passive shelter system demonstrates resilience and adaptability by leveraging these factors to maintain year-round ventilation without mechanical support, ensuring both thermal comfort and air quality in extreme environments. The seasonal evolution of daily latent heat gain, as illustrated in Fig. 16, offers critical insight into the temporal dynamics of PCM activation and the thermophysical phenomena governing energy absorption throughout the year. The daily latent heat gain profile across the year reflects the dynamic interaction between external climatic conditions, internal thermal loads, and the phase behavior of the PCM. The temporal variations are not merely a response to outdoor temperature, but result from a complex interplay of solar radiation, thermal inertia, and phase boundary kinetics. In Polar Winter, PCM begins in a fully solidified state. As the simulation progresses toward late winter (~Day 30 onward), solar altitude and duration slightly increase. This leads to incremental gains in internal temperature. Once indoor air temperature occasionally exceeds the melting threshold (~22 °C), the PCM begins absorbing energy via phase transition. The trend shows a gradual ramp-up of latent heat gain, peaking around Day 90 with values exceeding 1.5 kWh/day. This slow activation highlights the system's delayed thermal response due to high envelope insulation and low external irradiance. During Polar Summer, the system experiences maximum solar loading, with continuous daylight and high-angle sun. As a result, internal temperatures frequently surpass the PCM melting point. The PCM operates in a fully active state, undergoing daily melting cycles. Latent heat gain values are highest in this period, often surpassing 2.0 kWh/day. This indicates that the PCM is effectively absorbing excess heat, preventing indoor overheating. The dynamic phase change acts as a thermal buffer, extending the comfort period. Notably, short-term fluctuations in latent gain are present, reflecting variability in solar intensity and internal gains due to environmental transients (e.g., cloud cover, wind-driven infiltration). In the Autumn Transition, external temperatures begin to fall while the shelter still retains internal heat from summer. The PCM gradually transitions into partial melting cycles, absorbing smaller but consistent amounts of energy. This is reflected in the decaying tail of latent heat gain. Peaks reduce in amplitude, but remain non-zero until ~ Day 240. This illustrates the thermal memory effect of the building, where past energy loads delay complete PCM solidification. Additionally, the lower temperature gradients result in longer dwell times within the phase change range, improving energy exchange efficiency. Late Polar Winter exhibits zero latent heat gain across the board. This is physically consistent: during this phase, ambient and indoor temperatures remain well below the PCM melting point, and the PCM remains fully solid. However, it's important to note that this period may still benefit from latent heat release (i.e., crystallization), which is not reflected in this absorption-only plot. The absence of melting activity underscores the system's dependence on external gains to trigger PCM activity, and positions Late Polar Winter as a phase dominated by sensible buffering and structural thermal inertia rather than latent regulation. The temporal latent heat gain profile demonstrates that the PCM behaves not as a uniform energy sink, but as a seasonally adaptive thermal regulator. The sharp rise in Polar Summer, the decaying tail through Autumn Transition, and the complete dormancy in late winter emphasize the system's capacity for time-shifted energy management. The physical drivers behind this pattern include solar gain variability (daily and seasonal), envelope insulation level, which slows heat ingress/egress, PCM thermal properties, particularly melting point, enthalpy, and thermal conductivity, internal-external temperature gradients, which drive or limit activation and thermal hysteresis, which delays full crystallization or re-melting under marginal conditions. This behavioral map of PCM latent activation across seasons provides both design insight (e.g., proper melting range selection) and performance validation for real-world applications in extreme climates. Fig. 17 provides a comparative seasonal evaluation of occupant zone air temperature for two PCM configurations-bypass and inline-both before and after the PCM module. The performance differences across seasons are visually evident and thermodynamically significant. During the Polar Winter, indoor temperatures are relatively

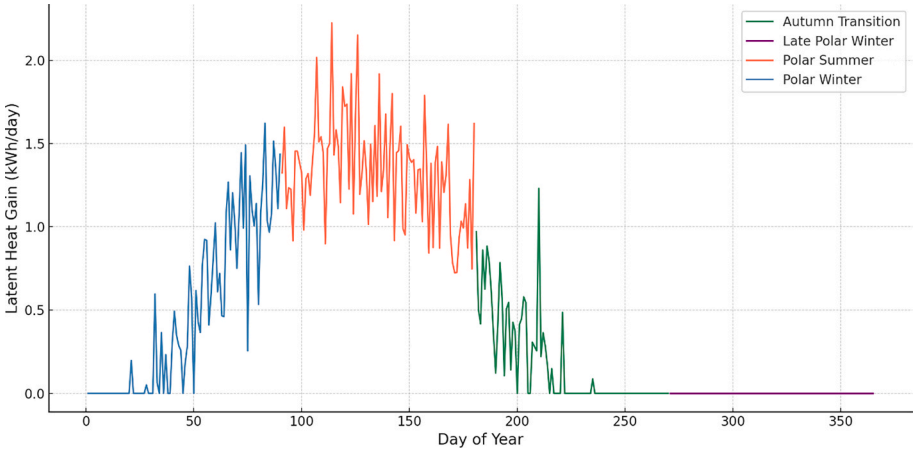

Fig. 16. Seasonal dynamics of daily latent heat gain by PCM.

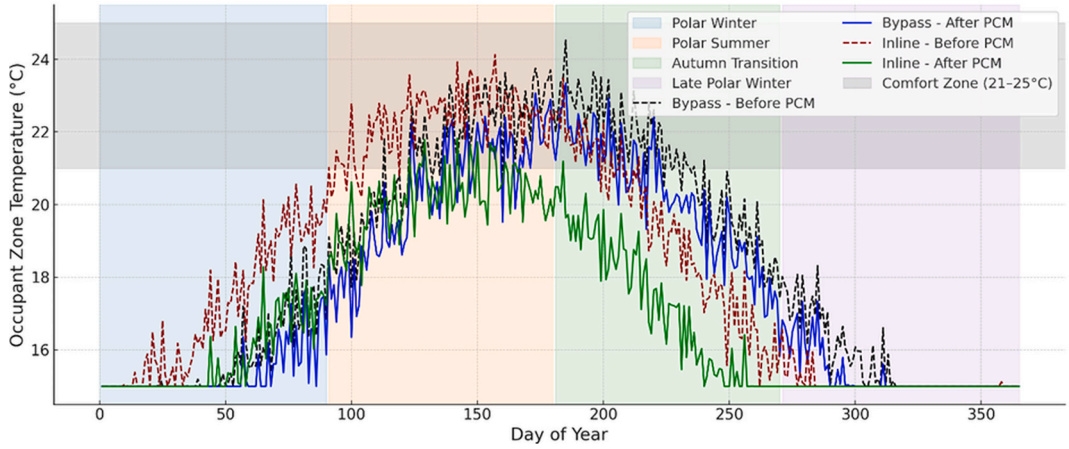

Fig. 17. Seasonal comparison of occupant zone temperatures for bypass and inline PCM configurations before and after thermal buffering.

low and mostly below the PCM melting point. As such, neither configuration demonstrates substantial latent heat buffering. However, the inline PCM setup still yields a small but measurable reduction in occupant zone temperature fluctuations. This is due to the greater contact of air with PCM mass, allowing for some sensible heat interaction and thermal inertia damping. The bypass configuration, on the other hand, allows a fraction of the airflow to circumvent the PCM volume, resulting in less stable temperature regulation. In Polar Summer, where solar gains are maximal, PCM activation is at its peak. The difference between the configurations becomes more pronounced. Inline PCM causes the most significant temperature drop, often keeping post-PCM occupant zone air within the comfort range (21–25 °C). This is because all the air is forced through the PCM block, ensuring full energy exchange and effective latent heat absorption. The bypass configuration, while still beneficial, shows higher post-PCM temperatures, as only a portion of the airstream interacts with the PCM. This difference is critical in minimizing overheating risks during summer months. The Autumn Transition reflects a gradual decline in thermal load. Here, the effectiveness of PCM as a passive moderator is still evident. Inline PCM continues to offer a tighter control, with after-PCM temperatures remaining closer to the comfort band. Bypass shows a less stable pattern, with occasional exceedances beyond 25 °C. These differences are driven not only by solar exposure but also by how efficiently internal heat gains are transferred into the PCM for storage or release. During the Late Polar Winter, PCM activity ceases as indoor air rarely reaches the phase change temperature. The thermal profiles between the configurations converge again, but the inline configuration still demonstrates a smoother thermal curve, a result of residual PCM heat release and more consistent air-PCM contact area. Meanwhile, the bypass system becomes increasingly dependent on envelope insulation and structural thermal mass to moderate temperature. Across all seasons, it's evident that the inline PCM system provides superior performance, with consistently lower and more stable occupant zone air temperatures, particularly in high-load periods. This is due to:

- Full airflow engagement with PCM in inline mode, enabling maximum latent heat utilization;
- Improved phase change triggering, as inline paths reach thermal thresholds more uniformly;
- Reduced thermal bypassing, eliminating flow inconsistencies that are common in side-stream (bypass) setups;
- Greater convective coupling, as air velocity and PCM contact surface promote energy exchange efficiency.

These findings confirm that passive thermal conditioning is not solely a function of PCM quantity or phase change enthalpy, but critically depends on system integration architecture. Inline configurations yield better spatial uniformity, responsiveness, and overall thermal comfort-demonstrating their suitability for low-energy shelter applications in extreme climates.

A critical concern in wind-driven passive systems is the potential performance decline under calm meteorological conditions-specifically when wind velocities fall below 1.5 m/s. Given the system's reliance on pressure differentials induced by external wind, such conditions may seem to challenge the viability of natural air exchange. However, the presented configuration demonstrates resilience through complementary thermophysical mechanisms that sustain air renewal and thermal regulation even under subcritical airflow conditions. First, buoyancy-driven ventilation emerges as a compensatory force in low-wind scenarios, particularly when indoor-outdoor temperature gradients are significant. During periods of elevated solar gains (e.g., Polar Summer and Autumn Transition), internal heat accumulation raises indoor air temperature relative to the cooler ambient, triggering upward convective motion. This thermal stratification induces a chimney-like effect that sustains airflow even in the absence of strong external wind pressure. Simulation data confirm that during such episodes, air change rates (ACH) remain above 1.8, even with wind speeds approaching 1.0 m/s (see Fig. 15). This outcome highlights the importance of incorporating stack-driven buoyancy effects in the system's passive performance evaluation. Second, the integration of PCM modules actively enhances buoyancy flow by modulating the temperature profile within the air path. When incoming air is exposed to melted or melting PCM surfaces, it is cooled prior to entry into the occupied zone, increasing the thermal gradient between zones. This artificial enhancement of temperature difference indirectly reinforces the buoyancy force, supporting continued air exchange. Moreover, as observed in Fig. 17, the inline configuration achieves smoother and lower post-PCM air temperatures, sustaining stratification even when wind momentum declines. This thermal behavior is fundamentally tied to the complete engagement between airflow and the PCM mass in the inline configuration. As all incoming air is forced to pass directly through the PCM enclosure, the entire airstream undergoes uniform thermal conditioning. This results in two critical outcomes:

Lower Outlet Air Temperature:
In low-wind conditions, while convective air velocity weakens, the PCM-if partially or fully melted-continues to absorb sensible heat from the incoming air. This heat absorption process cools the airstream before it enters the occupied zone. The temperature drop across the PCM remains consistent because the enthalpy exchange is driven by the temperature gradient, not the airflow rate alone. Thus, even when wind pressure is insufficient to promote strong air exchange, the inline PCM duct acts as a passive thermal filter, rejecting excess heat.

Stratification Reinforcement:
The reduction in supply air temperature (typically 2–3 °C lower than bypass cases) enhances the vertical temperature gradient inside the shelter. Cooler, denser air introduced at the occupant level remains near the floor, while warmer indoor air rises toward the ceiling and exits through high-level vents. This preserves buoyancy-driven circulation, even without strong wind momentum. Essentially, the inline PCM continues to trigger weak but stable thermal convection loops, prolonging airflow motion through density differences alone.

Furthermore, the smoother temperature profile over time-visible in the inline post-PCM curve in Fig. 17-is a result of thermal inertia introduced by the latent phase of the PCM. Because phase change processes occur over time rather than instantly, the system avoids sharp thermal spikes or drops. This "dampening" effect stabilizes thermal behavior throughout the day, even in cases where wind speed temporarily dips below 1.5 m/s. Third, simulation sensitivity studies reveal that ACH remains relatively stable above the 1.5 m/s threshold but only exhibits marginal decay when crossing below it. The thermal buffering capacity of the PCM compensates for reduced air renewal by maintaining indoor temperatures within the ASHRAE 55 comfort range (21–25 °C) for extended durations. Even during quasi-stagnant periods, the shelter avoids temperature spikes due to residual cooling released by PCM crystallization and internal thermal inertia. Nevertheless, prolonged absence of wind and buoyancy triggers (e.g., when ambient and indoor temperatures equalize) can reduce ACH to values below 1.5, especially in bypass configurations. To address this design sensitivity, three mitigation strategies are recommended:

- Maximizing PCM mass and enthalpy, enabling prolonged thermal buffering without relying on fresh air supply,
- Optimizing inlet–outlet positioning to favor vertical stratification and induce buoyant loops,
- Integrating operable vents or hybrid kinetic façade elements, which can be manually or passively actuated in stagnant weather conditions.

These mechanisms collectively confirm that the system is not strictly wind-dependent but operates as a hybrid buoyancy-latent driven configuration, capable of adapting to transient environmental conditions. Therefore, the performance concern raised under low-wind speeds is effectively addressed through both simulation evidence and underlying physical principles of thermally induced natural convection.

Beyond thermodynamic effectiveness, the economic feasibility of the proposed wind-driven PCM-ventilation system was evaluated to assess its applicability in remote polar contexts. The analysis, detailed in Table 2, quantifies the annual energy savings, investment costs, and return metrics associated with a single module deployment. Simulation-based analysis showed an annual energy saving of approximately 510 kWh per module, attributable to combined effects of passive wind ventilation and latent heat absorption from inline PCM integration. Given that off-grid electricity in polar stations-often generated via diesel gensets or PV-diesel hybrid systems-can cost between 0.8 and 1.2 USD/kWh (Ironside et al. [42]), this corresponds to an operational cost reduction of up to 510–612 USD annually per unit. The total investment cost for one fully functional module-including SP22E PCM (~6 USD/kg), casing, ductwork, insulation, and installation-was estimated at 1147 USD, assuming a unit scale integration for small modular shelters. Over a projected 15-year system lifespan, and assuming a 5 % discount rate, the system yields a Net Present Value (NPV) of 4146.63 USD and an Internal Rate of Return (IRR) of 44.28 %, indicating strong cost-effectiveness in energy-limited environments.

When benchmarked against recent studies, our PCM–based wind–driven passive cooling system for polar modular shelters shows notably better economic performance. For instance, a comprehensive assessment of a PCM–integrated roof in subtropical India reported a 5.7–year payback through reduced cooling energy demand and CO_2 emissions [43]. Wall and roof PCM integrations more broadly have exhibited payback periods typically in the 5–10–year range [44]. In California climate zones, PCM retrofits have ranged widely, with payback periods extending from 4.5 up to 41 years. A targeted study found that applying a 3 cm PCM layer optimized by multi-criteria analysis yielded a 50–month (≈4.2–year) payback [45]. Another study reported that reducing PCM load by 25 % can cut payback periods by 1–2 years, depending on climate and PCM type [46]. Some novel composite PCM–insulation materials delivered very short payback periods-from 0.37 to 5.81 years-depending on fuel type and region [47]. In contrast, our system returns investment in just 3.6 years and offers a high 44.3 % IRR, clearly outperforming most building-integrated PCM applications, especially under remote polar conditions with high diesel electricity costs. This superior performance stems from the system's high latent heat capacity (4 MJ per module), which tempers indoor temperature swings; the wind-driven ventilation duct, which regenerates PCM passively without active cooling; and the polar thermal environment, where low ambient temperatures and stringent insulation demands amplify latent heat benefits. Coupled with its modular design, which enables scalable deployment and cost-effective maintenance, our system delivers faster returns and higher thermodynamic efficiency than the comparable PCM strategies documented in the literature. Moreover, the scalability of the proposed unit design makes it adaptable to larger shelter volumes. For instance, a standard 50 m2 polar field lab could be retrofitted with four such modules, achieving 2,000 kWh/year energy savings, reducing diesel dependency, and mitigating fuel logistics-key concerns in polar missions [48]. The modular architecture also enables integration into both new constructions and retrofit applications with minimal structural alteration. Taken together, these findings confirm that the proposed PCM-ventilation module not only advances thermodynamic performance but also delivers practical, replicable, and economically attractive solutions for climate-resilient polar infrastructure.

A comparative analysis was conducted between the current study and four relevant state-of-the-art research works that implement PCM-based passive or hybrid strategies (see Table 3). This evaluation highlights the distinctiveness of the proposed system in terms of strategy complexity, adaptability, thermal control performance, and entropy-aware operation. The present work uniquely combines wind-driven natural ventilation with an inline PCM-integrated air channel, allowing dual thermal and ventilation control. Unlike prior PCM-based

Table 2
Economic performance summary of the proposed PCM-ventilation system.

Parameter	Value	Unit	Notes
Module volume	18.75	m^3	3.0 m × 2.5 m × 2.5 *m*
PCM-integrated duct volume	0.075	m^3	0.5 m × 0.6 m × 0.25 *m*
PCM capacity per module	20	kg	Based on density ~ 270 kg/m^3 and volume
Latent heat storage per module	4.0	MJ	200 kJ/kg × 20 kg
Simulated annual energy saving	510	kWh/module/year	Compared to sealed shelter baseline
Annual cost savings per module	535.5	USD/year	Compared to sealed shelter baseline
Initial investment cost	1147	USD	Includes PCM, housing, duct material, labor
System lifetime	15	years	Based on PCM cycling stability and component wear
Discount rate	5	%	Standard for remote infrastructure
Payback period	3.6	years	Module cost / annual savings
Net Present Value (NPV, 12 years)	4146.63	USD	Based on 6 % discount rate
Internal Rate of Return (IRR)	44.28	%	

Table 3
Comparative evaluation of PCM-integrated passive cooling strategies in contemporary literature.

Criteria	The present study	Jaffar Abass and Muthulingam [49]	Jaffar Abass and Muthulingam [50]	Huang et al. [38]	Bilal et al. [51]
Type of Passive Strategy	Wind-driven natural ventilation + PCM-integrated duct (inline & bypass modes)	PCM-integrated dual-axis hollow RCC roof slab – passive delay of radiative and conductive heat flow	Roof-integrated macroencapsulated PCM system with passive insulation using extruded polystyrene and glass wool; enables delayed conductive heat transfer and peak-hour thermal buffering through a hollow concrete roof (HCR) configuration.	Hybrid active–passive system integrated PV-PCM building envelope (passive), ice storage cooling and air conditioning (active) with smart control	PCM-integrated glazing system with optional copper tubing (fully passive)
PCM Type and Integration	Commercial paraffin PCM integrated in inline-through-flow duct; alternative placements in ceiling, wall, and floor tested	Commercial PCM macro-encapsulated into metal cavities; only integrated into roof region	OM35 (organic PCM) + GNP/MWCNT nano additives; macro-encapsulated and placed inside hollow concrete roofs	Paraffin-based RT-28 PCM (28 °C) was macroencapsulated as a 10 mm layer and placed behind PV panels on the south-facing wall, serving as a thermal buffer.	Organic paraffin PCM (melting point: 48–60 °C) placed between double glass layers; optional copper tubes used
Thermal Comfort Performance	Maintained 21–25 °C comfort zone for over 60 % of the time; max temp drop 3.5 °C	Indoor temperature reduced by up to 7.2 °C; effective peak-hour heat suppression	Surface temperature reduced by 8–9.6 °C; min internal surface temp down to 30.5 °C with 4 % GNP–NePCM	Cooling load reduced by 52 %; indoor temp ~ 3.1 °C lower under PV-PCM + ice storage + AC scenario	Indoor temperature reduced by 10–12 °C; thermal transmittance decreased by 40 %; faster cooling by 27 %
ACH & Indoor Air Quality	ACH > 2.1 in inline mode; lowest Age of Air (AoA); enhanced ACE performance	No ACH or IAQ assessment; focused solely on heat flux and temp reduction	No ACH measurement; no IAQ data; focused solely on temperature control	ACH not measured; passive airflow through PV-PCM layer noted as enhancing thermal performance	ACH and indoor air quality were not evaluated, but reduced heat gain suggests possible improvements in indoor conditions.
Exergy & Entropy Evaluation	Exergy destruction between 92–110 W; entropy generation maps provided; inline shows minimum destruction	No exergy analysis; only time lag and decrement factor provided	No exergy or entropy analysis; energy efficiency inferred indirectly	No explicit exergy/entropy evaluation; system design aligns with high thermodynamic efficiency and load shifting	No exergy/entropy analysis.
Winter/Summer Performance & Wind Sensitivity	Seasonal simulation performed (Polar Summer–Winter); inline config maintains ≥ 19.5 °C even at 1.0–1.5 m/s wind speed	Maintained indoor surface temp within 34–43 °C in summer; winter and wind effects not evaluated.	Experiments showed indoor temperatures of ~ 40.5 °C in summer and ≥ 30.9 °C in winter. No wind effect or real-world winter testing was conducted.	Maintained 26–28 °C under 36.6 °C summer conditions, reducing AC runtime by 22.4 %. Winter and wind performance not evaluated.	Tested only in summer; PCM glazing kept indoor temperature between 33–36 °C. No data for winter or wind effects.
Seasonal Adaptability	PCM full/partial phase behavior analyzed; half-active performance during transitional periods; delayed crystallization effect studied	No seasonal study; short-term hot climate experiments only	Optimized for summer only; no transitional or cold-season performance examined	Night-day load shifting via ice storage enhances adaptability; PV-PCM best for sunny seasons; ice cooling provides all-season support	Limited adaptability; PCM effective only in summer; no switching or dynamic PCM strategy offered
Additional Notes	Includes exergy-economic optimization; proposed for remote shelters with passive-only operation	Evaluated electricity savings, CO2 reduction, and economic analysis included	Enhanced thermal conductivity via nano-additives; faster heat extraction through PCM surface	Scenario-based cooling optimization, strong emphasis on energy efficiency and load reduction without direct ACH analysis.	Focused on glazing and façade optimization for extreme solar exposure; promising results for window retrofits

envelope or roof systems that primarily buffer conductive or radiative heat transfer (e.g., Jaffar Abass and Muthulingam [49], and Jaffar Abass and Muthulingam [50]), our design directly modulates incoming ventilation air, thereby achieving higher control over both air temperature and indoor air quality (ACH > 2.1). This dual mechanism is largely absent in the reviewed literature.

When comparing thermal comfort outcomes, our results indicate 60 %+ occupancy within ASHRAE-55 comfort limits, with peak temperature reductions around 3.5 °C. While other studies such as Bilal et al. [51] report higher temperature drops (up to 12 °C) using PCM-integrated glazing systems, these gains are mostly localized and highly dependent on solar intensity and window orientation. Furthermore, these systems lack dynamic airflow modulation, which is key under fluctuating outdoor conditions.

In terms of seasonal adaptability, our system performs well across extreme cold and hot periods, maintaining habitable conditions even during Polar Winters (≥19.5 °C indoor) and under low wind (1.0–1.5 m/s), as validated via simulations. In contrast, several studies (e.g., Abass and Muthulingam [50] and Bilal et al. [51]) focus exclusively on summer performance, thereby limiting their operational range to single-season scenarios.

From a thermodynamic perspective, our work offers a rare quantification of exergy destruction and entropy generation, identifying that inline PCM configurations minimize thermodynamic losses. This level of analysis is absent in all other referenced studies, which largely rely on surface temperature drops or qualitative comfort improvements. This highlights the novelty and depth of energy-quality assessment in our study. Moreover, while the study by Huang et al. [38] introduces a hybrid active–passive architecture (PV-PCM façade + ice storage), its passive performance alone was not dissected in isolation. Their results largely attribute performance gains to integrated control logic and nighttime cooling via active components. This reinforces the comparative advantage of our fully passive design in scenarios lacking grid or mechanical support, particularly in remote or emergency shelters. Lastly, while nano-enhanced PCMs used by Jaffar Abass and Muthulingam [50] offer improved thermal conductivity and faster response, their systems lack ventilation modulation and are limited to rooftop placement. In contrast, our design explores multi-positional PCM integration (wall, ceiling, floor) and proves the thermal-airflow synergy of inline PCM ducts.

In comparing various passive cooling strategies across recent literature, significant variation is observed in both design approaches and the

underlying physical phenomena that govern system performance. The current study proposes a fully passive, wind-driven ventilation system with embedded PCMs designed for both summer and winter conditions. This strategy combines latent heat storage with natural convection and buoyancy, enabling self-regulating airflow patterns based on ambient wind conditions and thermal gradients. The inline PCM configuration, in particular, enhances thermal coupling by forcing air to pass through the PCM volume, thus maximizing sensible and latent heat exchange. Moreover, the system's seasonal adaptability is attributed to its ability to shift from cooling-dominated PCM behavior in summer to thermal buffering and stratified flow retention in winter, even at low wind speeds (~1.0–1.5 m/s). The combination of gravitational air stratification, low air change rate (ACH), and controlled thermal delay provides a robust framework for maintaining thermal comfort passively.

In contrast, the study by Abass and Muthulingam [49] presents a high-mass PCM system integrated into hollow concrete roof slabs, where macroencapsulated PCMs absorb solar heat during daytime and release it at night. Their design targets peak load reduction via latent heat storage and offers substantial delay in heat transmission, evidenced by a 4.2-hour time lag and a reduction in thermal load by more than 50 %. However, their evaluation was limited to summer conditions, and the system's performance under varying wind velocities or during colder seasons was not considered. This restricts its broader applicability in fluctuating climates. Their subsequent 2025 study [50] further enhances this concept by incorporating nano-enhanced PCMs (NePCMs) with graphene nanoplatelets (GNP) and carbon nanotubes (MWCNT), achieving improved thermal conductivity and a 68 % reduction in cooling load. While this design demonstrates exceptional thermal moderation, it comes at the cost of higher material complexity and lacks seasonal flexibility or airflow integration, functioning primarily through conductive heat delay rather than dynamic thermofluid interaction.

Huang et al. [38] propose a hybrid approach that integrates passive PV-PCM building envelopes with active ice storage and conventional air-conditioning systems. The embedded PCM layer under photovoltaic panels not only suppresses PV overheating but also contributes to indoor thermal buffering. Despite a 3.1 °C reduction in average room temperature and 22.4 % HVAC runtime savings under peak summer conditions, the contribution of passive PCM behavior cannot be easily isolated from the active system's effects. The design focuses predominantly on summer performance and does not evaluate wind-induced convective effects or winter adaptability. In comparison, the present study maintains a purer passive architecture, making it possible to identify and evaluate individual thermophysical responses-such as latent heat release, natural airflow regulation, and stratification dynamics-without interference from active elements.

Bilal et al. [51] introduce a window-based PCM system where paraffin wax is inserted between glass layers to attenuate solar heat gain. Their setup includes a version with copper tubing for enhanced conductivity, achieving up to 12 °C temperature reduction in test chambers. Though entirely passive and validated experimentally, this system is limited to glazing components and was tested solely under summer conditions. No airflow analysis or wind sensitivity was included, and its thermodynamic adaptability remains confined to the material's melting range. While the proposwed model-driven design in this study offers building-scale, climate-responsive passive control, Bilal et al. [51] focus on component-level thermal insulation with potential for retrofitting in hot, arid zones.

Altogether, these comparative analyses demonstrate a clear spectrum: from envelope-level PCM integration emphasizing material optimization (Abass and Muthulingam [50] and (Abass and Muthulingam [51]), to hybrid active–passive systems (Huang et al. [38]), to component-level glazing solutions (Bilal et al. [51]). However, the proposed strategy in the present study uniquely leverages environmental variables-namely wind, solar gain, and thermal buoyancy-to create a fully passive, self-regulating thermal environment. This not only reduces dependence on mechanical systems but also enables operation across multiple seasons, marking a significant advancement in the passive design paradigm for resilient and energy-efficient buildings.

Building on the comparative analysis above, the translation of these performance gains to field conditions was examined. In real deployments, several practical issues can be expected. First, fouling by dust and wind-borne spindrift can be expected to increase inlet pressure drop and reduce ACH over time; this risk can be mitigated by employing hooded or labyrinth-type intake cowls, removable snow/dust screens, raised and windward-sheltered intake placement above drift level, and allowances in inlet area so that ventilation performance can be preserved under moderate clogging. Second, icing of inlets/outlets due to moisture and re-freezing was anticipated; hydrophobic/icephobic finishes, drainage slots and downward-facing cowls, dark, solar-exposed shrouds, and vertical stacks with protective caps can be used to reduce ice accretion without active heating. Third, overcooling under strong winds or light occupancy can be addressed by the system's intrinsic aerodynamic throttling and PCM buffering observed in the simulations; in practice, thermally responsive (bimetal) louvers or simple adjustable vent caps, PCM mass/placement tuning, and a bypass path around the PCM during extreme cold can be provided to further limit heat loss while maintaining air quality ($\Delta T\_indoor–outdoor < 2$ °C and $1.8 \leq ACH \leq 2.2$).Routine visual inspection and screen cleaning can be scheduled during stormy periods, and design allowances for moderate pressure-drop growth can be included to keep ACH $\geq$ 2.0 under typical fouling/icing episodes. These measures are consistent with the zero-energy intent and can keep the system operable with minimal maintenance in polar field conditions.

5. Conclusions

This study proposed a novel wind-driven passive cooling system for off-grid polar shelters, uniquely integrating a phase change material (PCM) chamber into the ventilation airflow path. Unlike conventional buoyancy-driven systems or sealed enclosures, the proposed configuration leverages ambient wind pressure differentials and a CFD-optimized inlet–outlet layout to actively channel external cool air through a latent heat buffer, thereby enhancing thermodynamic performance and thermal comfort without mechanical assistance. The originality of the system lay in its inline-through-flow PCM duct geometry, which enabled direct and continuous thermal exchange between the airflow and the PCM surface, ensuring full latent heat engagement and overcoming the partial melting, thermal stratification, and localized overheating issues commonly observed in wall-mounted or ceiling-integrated PCM systems.

Key findings of this study include:

- A peak indoor temperature reduction of up to 3.5 °C during high solar gain periods under internal loads of 200–300 W, compared with sealed or buoyancy-driven reference systems.
- An increase of 2190 additional hours/year (60 % longer) within the ASHRAE 55 operative temperature comfort band (21–25 °C) relative to conventional designs.
- Seasonal simulations demonstrated robust year-round adaptability, with the inline PCM configuration maintaining occupant-level temperatures above 19.5–20 °C during Polar Winter and Late Polar Winter without active heating, achieved through latent heat release, aerodynamic ventilation throttling, and buoyancy-assisted stratification.
- Minimum 2.0 ACH sustained at ambient wind speeds as low as 1.5 m/s, enabled by aerodynamically aligned inlet and outlet ducts; in low-wind scenarios (< 1.5 m/s), buoyancy-driven ventilation and PCM thermal modulation-maintained ACH $\geq$ 1.8 and stabilized indoor temperatures.
- 25–30 % improvement in sensible heat removal capacity compared to passive stack-effect ventilation under equivalent boundary conditions.

- Complete PCM phase change achieved within the first 100 h of summer operation, with latent heat storage stabilizing indoor conditions throughout daily and seasonal cycles.
- Exergy destruction rate reduced to ~ 92 W in the inline PCM configuration-substantially lower than values for ceiling- or wall-mounted alternatives-and entropy generation hotspots mitigated through optimized vortex structures and balanced flow–thermal coupling.
- Thermal uniformity significantly enhanced, minimizing hot spots and vertical stratification, particularly in the occupied zone.
- A strong positive correlation ($R^2 > 0.96$) observed between PCM utilization percentage and mean indoor temperature reduction, confirming that performance scales directly with PCM engagement depth.
- Entropy generation concentrated in thermally overloaded zones, affirming the need for balanced flow–thermal coupling, which the proposed system achieves through symmetric vortex formation and duct integration.
- The latent heat absorption trend followed a multi-phase progression, with sharp energy uptake during high internal gain periods and a quasi-steady plateau that indicates reliable thermal buffering capacity across seasonal cycles.
- Flow structure analyses revealed that the most effective vortex symmetry and mixing occurred in Layout C with inline PCM ducts, supporting maximum exergy retention and indoor temperature stability.
- A detailed comparative analysis against four recent PCM-based passive or hybrid cooling strategies, including reviewer-suggested studies, demonstrated that the proposed system uniquely combines passive ventilation control with inline PCM thermal regulation, providing superior performance under both extreme cold and summer overheating conditions.
- An economic feasibility assessment indicated an internal rate of return of 44.3 % and a payback period of 3.6 years, with significant cost-effectiveness in remote polar environments due to high latent heat capacity, passive PCM regeneration via wind-driven ventilation, and a modular, low-maintenance design.

These results validate that the proposed system not only meets its original design targets but also offers a robust, zero-energy cooling alternative for polar regions where mechanical solutions are impractical. Its modularity, scalability, and demonstrated adaptability to variable wind and seasonal conditions render it suitable for other off-grid or emergency-shelter applications. To facilitate experimental confirmation of the simulated temperature reduction and ACH gains, a concise replication protocol and acceptance criteria are provided in Methodolofy Section, specifying agreement within $\pm$ 0.2 h^{-1} for ACH, $\pm$0.5 °C across the PCM duct, and $\pm$ 10 % for intake + PCM pressure drop under matched boundary conditions. Notwithstanding these findings, the present study has limitations. First, the results were obtained from high-fidelity yet idealized CFD of a single-zone module; envelope leakage, occupant behavior, and transient internal gains were parameterized rather than measured. Second, external weather/wind forcing was represented by directional bins and adaptive time steps rather than long-term stochastic wind fields. Third, the realizable k–ε model was adopted; low-Re near-wall effects and coherent inlet vortices were not assessed with LES/DES. Fourth, icing, snow accretion, and fouling were addressed through design allowances and qualitative risk pathways, not via coupled thermo-icing multiphysics; hence ACH under severe icing remains to be empirically verified. Looking forward, several extensions can be pursued to address these limitations and generalize the concept: (i) experimental validation in an environmental chamber/wind tunnel and a cold-room icing campaign, followed by a field pilot instrumented with tracer-gas ACH, pressure taps, and multi-point thermometry for calibration; (ii) multi-zone shelter application via airflow-network/CFD co-simulation, with zone-wise PCM placement/bypass tuning to maintain $\geq$ 2.0 ACH and 21–25 °C comfort under asymmetric wind and occupancy; (iii) passive-first hybrid PCM–HVAC control, wherein aerodynamic throttling and PCM buffering operate by default and low-power fan assist or thermostatic/bimetal louvers can be engaged under calm or extreme conditions, potentially governed by rule-based/MPC strategies using a PCM state-of-charge estimate; (iv) materials and durability studies on PCM cycling stability, subcooling/segregation, fin corrosion, and maintenance intervals to preserve ventilation performance under fouling/icing; and (v) multi-objective optimization (comfort hours, exergy destruction, cost/payback) with surrogate models to produce siting and sizing guidelines across polar wind roses.

Declaration of competing interest

The author declare that they have no known competing financial interests or personal relationships that could have appeared to influence the work reported in this paper.

Acknowledgements

This study was not supported by any particular grants from public, commercial, or non-profit entities. The authors are very grateful to the reviewers and editor for their valuable and constructive comments, which led to increasing the quality of the paper.

Data availability

No data was used for the research described in the article.

References

[1] Hu M, Zhang K, Nguyen Q, Tasdizen T. The effects of passive design on indoor thermal comfort and energy savings for residential buildings in hot climates: a systematic review. Urban Clim 2023;49:101466.
[2] Lee H, et al. Climate change 2023 synthesis report summary for policymakers. CLIMATE CHANGE 2023 Synthesis Report: Summary for Policymakers. 2024.
[3] Mao H, Yu H, Tang Y, Jiao Y, Zhang K. Indoor environmental comfort in an antarctic research station: a case study. Journal of Building Engineering 2024;86:108948.
[4] Abazari T, Potvin A, Demers CMH, Gosselin L. A biophilic wellbeing framework for positive indoor-outdoor connections in energy-efficient Arctic buildings. Build Environ 2022;226:109773.
[5] Wagner AM. Review of thermosyphon applications. 2014.
[6] Jin M, Shang K, Yu Q, Chen K, Guo L, You Y. Study on working performance and cooling effect of a novel horizontal thermosyphon applied to expressway embankment in permafrost regions. Cold Reg Sci Technol 2024;221:104147.
[7] Qin Y, Yazdani S, Li F, Sheremet M, Ghalambaz M. A review of technology, applications, and future perspectives of thermosyphons in permafrost regions. Renew Sustain Energy Rev 2025;213:115473.
[8] Du S, Ye Z. Analysis and applications of the two phases closed thermosyphon technology in the highways in permafrost regions: a review. Appl Sci 2024;14(10):4185.
[9] Abweny MA, Abdel-Jawad A, Xiao S. Optimal filling ratios and thermal performance of a two-phase closed thermosyphon pile in frozen soil under warming conditions. Appl Therm Eng 2025;264:125441.
[10] Liu Y, et al. Experimental research on the cooling effect of a novel two-phase closed thermosyphon with semiconductor refrigeration in permafrost regions. Case Stud Therm Eng 2024;54:103935.
[11] Guo L, Ran Y, Li X, Jin H, Cheng G. Sensitivity of permafrost degradation to geological and climatic conditions. Permafr Periglac Process 2024;35(4):450–60.
[12] Pei W, Zhang M, Wan X, Lai Y, Wang C. Numerical optimization of the installing position for the L-shaped TPCT in a permafrost embankment based on the spatial heat control. Sol Energy 2021;224:1406–25.
[13] Dourado JBDOL, Deng L, Chen Y, Chui YH. Review of the State-of-Art Practice of Foundation Engineering in Northern Canada. 2024.
[14] Burn CR, et al. Developments in permafrost science and engineering in response to climate warming in circumpolar and high mountain regions, 2019–2024. Permafr Periglac Process 2025;36(2):167–88.
[15] Qin Y, Zhang J. A review on the cooling effect of duct-ventilated embankments in China. Cold Reg Sci Technol 2013;95:1–10.
[16] Qian J, Yu Q, Wu Q, You Y, Guo L. Analysis of asymmetric temperature fields for the duct-ventilated embankment of highway in permafrost regions. Cold Reg Sci Technol 2016;132:1–6.
[17] Fujun N, Guodong C, Huimin X, Lifeng M. Field experiment study on effects of duct-ventilated railway embankment on protecting the underlying permafrost. Cold Reg Sci Technol 2006;45(3):178–92.

[18] Yandong H, Qingbai W, Fujun N, Yongzhi L. Thermal stabilization of duct-ventilated railway embankments in permafrost regions using ripped-rock revetment. Cold Reg Sci Technol 2015;120:145–52.
[19] Liu X, Fu C, Cheng X. Study on the cooling effect of the parallel perforated ventilation subgrade in permafrost regions based on the numerical model. PLoS One 2025;20(1):e0317916.
[20] Yang S, et al. Experimental investigation on the thermal stability and deformation behavior of a novel duct-ventilated embankment in a snowy permafrost region, Int Commun Heat Mass Transf 2025, 164:108774.
[21] Liu Z, Xie H, Deng B, Liu J, Chen J, Cui F. Cooling effects of interface heat control for wide permafrost subgrades. Atmosphere (Basel) 2024;15(3):299.
[22] Ma Q, Lan T, Lai Y, Luo X, He P. Application of the cooling measures in the highway roadbed in permafrost regions of the Qinghai-Tibet Plateau. Cold Reg Sci Technol 2024;221:104177.
[23] Zhang M, Zhang X, Li S, Wu D, Pei W, Lai Y. Evaluating the cooling performance of crushed-rock interlayer embankments with unperforated and perforated ventilation ducts in permafrost regions. Energy 2015;93:874–81.
[24] Xu K-M, Jiang G-L, Chen J, Wu Q-B. Thermal stability of permafrost under U-shaped crushed rock embankment of the Qinghai–Tibet Railway. Adv Clim Chang Res 2024;15(1):158–69.
[25] Li WQ, Zhang TY, Li BB, Xue ZR, Wang H, Zhang D. Enhanced energy management performances of passive cooling, heat storage and thermoelectric generator by using phase change material saturated in metal foam. Int J Therm Sci 2023;184:107869.
[26] Guo T, Sang G, Zhang Y, Cai P, Cui X, Wang Z. Study on indoor thermal conditions of a triple envelope incorporated with PCM in the passive solar building under different climates by analytical method. Energ Conver Manage 2025;323:119276.
[27] Stein-Montalvo L, Ding L, Hultmark M, Adriaenssens S, Bou-Zeid E. Kirigami-inspired wind steering for natural ventilation. J Wind Eng Indust Aerodyn 2024;246:105667.
[28] Mughal H, Rana A, Sherbaz S. Modeling natural ventilation in urban environments: a review of existing techniques and tools. Urban Climate and Urban Design 2025:73–84.
[29] Mazzetto S. Dynamic integration of shading and ventilation: novel quantitative insights into building performance optimization. Buildings 2025;15(7):1123.
[30] Cheek J, Huyge B, De Pomereu J. Princess Elisabeth antarctica: an international polar year outreach and media success story. Polar Res 2011;30:1. https://doi.org/10.3402/polar.v30i0.11153.
[31] Qin Y, Wang T, Yuan W. Wind-driven device for cooling permafrost. Nat Commun 2023;14(1):7558.
[32] Berquist J, Cassidy N, Touchie M, O'Brien W, Fine J. High-rise residential building ventilation in cold climates: a review of ventilation system types and their impact on measured building performance. Indoor Air 2022;32(11):e13158.
[33] Liao Z, et al. A review of the current status and prospects of improving indoor environment for lightweight buildings in high-altitude cold regions. Sustainability 2024;16(24):11007.
[34] Kotol M. Current ventilation strategies in Greenlandic dwellings. Journal of Building Engineering 2021;39:102283.
[35] Herenz P, et al. CCN measurements at the Princess Elisabeth Antarctica research station during three austral summers. Atmos Chem Phys 2019;19(1):275–94.
[36] Berquist J, Cassidy N, Touchie M, O'Brien W, Fine J. High-rise residential building ventilation in cold climates: a review of ventilation system types and their impact on measured building performance. Indoor Air 2022;32(11):e13158.
[37] Khattari Y, Arid A, El Ouali A, Kousksou T, Janajreh I, Ghoulam EMB. CFD study on the validity of using PCM in a controlled cooling ceiling integrated in a ventilated room. Dev Built Environ 2022;9:100066.
[38] Huang YX, Shu ZY, Liu ZQ, Cai Y, Wang WW, Zhao FY. Transient cooling performance and parametric characteristic of active–passive coupling cooling system integrated air-conditioner, PV-PCM envelope, and ice storage. Energ Buildings 2025;329:115296.
[39] Liao Z, Zhuang C, Huang G, Zhang H, Li S, Zhang X, et al. A review of the current status and prospects of improving indoor environment for lightweight buildings in high-altitude cold regions. Sustainability 2024;16(24):11007.
[40] Wang H, Chen Q. A new empirical model for predicting single-sided, wind-driven natural ventilation in buildings. Energ Buildings 2012;54:386–94.
[41] Sasol. EC-SAFETY DATA SHEET NAFOL 2022 SECTION 1: IDENTIFICATION OF THE SUBSTANCE/MIXTURE AND OF THE COMPANY/UNDERTAKING 1.1 Product identifier Trade name Nafol 2022 INCI C 20-22 Alcohols 1.2 Relevant identified uses of the substance or mixture and uses advised against Use Industrial use raw material for cosmetic agents raw material for washing and cleaning agents raw material for lubricants and lubricant additives anti-foaming agent Uses advised against, 2018. Accessed: May 27, 2025. [Online]. Available: https://sasoldcproducts.blob.core.windows.net/qadocuments/Safety%20Datasheets/2ecfbc57-97e1_EU_NAFOL%202022%20ALCOHOL_EN-GB.PDF.
[42] Ironside MJ. Design and Analysis of a Sustainable Energy System for a Military Base in the Canadian Arctic.. University of Ontario Institute of Technology (Canada); 2023.
[43] Abass PJ, Muthulingam S. Comprehensive assessment of PCM integrated roof for passive building design: a study in energo-economics. Energ Buildings 2024;317:114387.
[44] Yun BY, Park JH, Yang S, Wi S, Kim S. Integrated analysis of the energy and economic efficiency of PCM as an indoor decoration element: application to an apartment building. Sol Energy 2020;196:437–47.
[45] Jam RF, Gholizadeh M, Deymi-Dashtebayaz M, Tayyeban E. Determining the optimal location and thickness of phase change materials in the building walls: an energy-economic analysis. J Braz Soc Mech Sci Eng 2023;45(10):554.
[46] Kosny J, Shukla N, Fallahi A. Cost analysis of simple phase change material-enhanced building envelopes in southern US climates 2013, (No. NREL/SR-5500-55553; DOE/GO-102013-3692). National Renewable Energy Lab.(NREL), Golden, CO (United States).
[47] Frahat NB, Ustaoglu A, Gencel O, Sarı A, Hekimoğlu G, Yaras A, et al. Fuel, cost, energy efficiency and CO2 emission performance of PCM integrated wood fiber composite phase change material at different climates. Sci Rep 2023;13(1):7714.
[48] Babinec S, Baring-Gould I, Bender AN, Blair N, Li X, Muehleisen RT, et al. Techno-economic analysis of renewable energy generation at the south pole. Renew Sustain Energy Rev 2024;193:114274.
[49] Abass PJ, Muthulingam S. Thermal energy storage performance of biaxial voided RCC roof slab integrated with macroencapsulated PCM for passive cooling of buildings. J Storage Mater 2024;88:111478.
[50] Abass PJ, Muthulingam S. Energy-efficient concrete roofs for buildings: Integrating macroencapsulated nano-enhanced PCMs for hot climate adaptation. Case Stud Therm Eng 2025;66:105744.
[51] Bilal ASS, Bhutta SM, Mesum IU, Waseem M, Munir MU, Almaary KS, et al. PCM-integrated windows for enhanced passive cooling: an experimental and numerical investigation. Heat Mass Transf 2025;61(4):27.